Electron-Phonon Interaction Effects in the Spectra of Hydrogenated, Deuterated, and Tritiated Crystals of Calcium and Strontium Fluorides Containing Cerium†

I. T. Jacobs, G. D. Jones, and K. Ždánský, *
Department of Physics, University of Canterbury, Christchurch, New Zealand

and

R. A. Satten
Department of Physics, University of California, Los Angeles, California 90024
(Received 17 November 1970)

Spectroscopic measurements of cerium-hydride, cerium-deuteride, and cerium-tritide ion pairs in calcium and strontium fluoride crystals are reported. The local-mode spectrum of the hydride ion shows a splitting of the doubly degenerate vibration which is attributed to electron-phonon interaction effects between the cerium $4f$ electronic states and the hydride-ion local-mode phonons. A dipole moment of $1.1ea_0$ for the hydride ion, where a_0 is the Bohr radius, is postulated to explain the observed local-mode spectrum. The electronic lines of the tetragonal cerium-hydride ion pairs display large isotope shifts of 23.8 and 35.1 cm^{-1} for hydrogen to deuterium and hydrogen to tritium, respectively. Only the nondegenerate vibration of the hydride ion appears in the vibronic spectrum of the $4f \rightarrow 5d$ transition of cerium and has a higher frequency when coupled to the cerium-ion $5d$ electronic state than to the $4f$ electronic states. The intensity of these vibronics relative to their parent electronic lines is quantitatively explained on a configuration-coordinate model. Both the electronic line isotope shifts and the vibronic frequency shifts are attributed to electron–local-mode-phonon interaction effects in the cerium-ion $5d$ electronic state. A quantitative model for the electron–local-mode-phonon interaction with point-charge and dipolar interactions between the cerium ion and the hydride ion is set up and includes anharmonic effects. This model successfully explains the vibronic splitting in the local-mode spectrum, the occurrence of only one local-mode frequency in the vibronic spectrum of the cerium $4f \rightarrow 5d$ transition, and the relative intensity of these lines, but is unsuccessful in explaining the magnitude or sign of the observed isotopic effects. The estimated electronic line isotope shifts are $\frac{1}{4}$ the magnitude of the observed shifts and of opposite sign.

I. INTRODUCTION

Negative hydrogen ions can be incorporated into alkaline-earth fluoride crystals in relatively high concentration, and the crystals then show infrared absorption due to localized modes of the hydride ion. In crystals containing trivalent rare-earth ions,[1] the hydride ions can serve as charge compensators for the rare-earth ions, and the coupling between the two ions manifests itself in several ways: (a) as a shift in the electronic levels of the rare-earth ion in the changed environment due to the hydride ion, (b) as an isotope effect for these shifted lines, and (c) as vibronic transitions involving the localized vibration modes of the hydride ion. The work here is concerned with the determination and interpretation of these coupling effects for the case of hydride-, deuteride-, and tritide-ion impurities in calcium and strontium fluoride crystals containing cerium.

The crystalline environment around a trivalent rare-earth ion is expected to have a greater effect on interconfigurational transitions than on transitions within the shielded $4f$ shell. This is because excited states such as $5d$ and $6s$ are not shielded from the surrounding ions. It is expected and found that the coupling effects above, previously reported for the lanthanon fluorides,[2] are considerably enhanced for $4f$-$5d$ transitions of the rare-earth ions, and it is possible to attempt quantitative calculations for these effects.

Cerium is a particularly suitable rare-earth ion for these investigations. In calcium fluoride the lowest $4f$-$5d$ transition is at 3100 Å, i.e., in a spectral region readily accessible to experimental study. This transition shows a well-developed fine structure in both absorption and fluorescence, comprising a zero-phonon line and an associated vibrational series consisting of the lattice vibrations of calcium fluoride superposed on a 484-cm^{-1} progression.[3] It has been shown that the cerium ion giving rise to this spectrum is situated in a tetragonal site with a charge-compensating fluoride ion in the nearest interstitial site.[4] Analogous spectra are observed for strontium and barium fluoride crystals containing cerium.

In this paper, the spectra of hydrogenated, deuterated, and tritiated crystals of calcium and strontium fluoride crystals containing cerium are reported. The spectra of the hydride, deuteride,

and tritide analogs of the fluoride-compensated site are identified and the various local-mode coupling effects observed in their spectra are discussed.

The principal part of this paper concerns the interpretation of the local-mode coupling effects in terms of the electron-phonon interaction between the cerium $4f$ and $5d$ electronic states and the hydride, deuteride, and tritide local-mode phonons. Both the point-charge model and dipole model for this interaction are developed and found to satisfactorily account for the main features of the spectra. The models are, however, conspicuously unsuccessful in explaining the isotope shifts occurring in the spectra when either deuterium or tritium substitutes for the hydrogen and other possible mechanisms for explaining these shifts are proposed.

II. EXPERIMENTAL TECHNIQUES

The calcium fluoride crystals containing cerium used in these investigations were purchased from the Hebrew University of Jerusalem, Israel. They were grown by the Stockbarger method from calcium fluoride and cerium fluoride. Oxygen was removed from the starting material by the use of lead fluoride as a scavenger. Most of the measurements were made on 0.05% concentration crystals. The corresponding strontium and barium fluoride crystals were purchased from Optovac, Inc.

The crystals were first heated under high vacuum at 500 °C in the presence of aluminum metal in a quartz tube. Hydrogen or deuterium gas was then introduced to two-thirds atmosphere pressure and the temperature raised to 800 °C for a period of 24 h. The crystals were then rapidly quenched by pulling the crystals out of the furnace to room temperature in about 1 min. In the case of tritium, the gas pressure used was one-tenth atmosphere, and the isotopic percentage achieved in the crystals averaged 20% tritium. These crystals darken with time as a result of irradiation by the tritium impurity present; the uniformity of the coloration shows that the tritium is uniformly distributed in the crystal.

Infrared measurements were made in the 4000–200-cm^{-1} range with a Beckman IR 12 infrared spectrophotometer. Low-temperature spectra were obtained with a metal Dewar in which the crystals were cooled by thermal contact with a copper block.

The absorption spectra of the cerium crystals were recorded photoelectrically on a Spex 1700 monochromator with an iodine quartz lamp as source. Low-temperature spectra were obtained using an Andonian variable temperature Dewar. Wavelengths of the absorption lines were measured to better than 0.2 Å. Low-resolution absorption spectra over the 2000–4000-Å spectral range were obtained with a Cary 14R spectrophotometer.

The fluorescence spectra were obtained photoelectrically on the Spex using a Philips high-pressure mercury lamp for excitation.

III. INFRARED SPECTRA

Calcium, strontium, and barium fluoride crystals have cubic symmetry (space group O_h^5). Each calcium or strontium ion is surrounded by eight fluorines at the corners of a cube, and every second cube of fluorines is empty. (Fig. 1). In the fluoride crystals containing rare-earth ions, charge compensation is required and in hydrogenated crystals the hydride ions may serve as charge compensators. It has been shown in previous work[1] that charge compensation of the trivalent rare-earth ion by a hydride ion located in an adjacent empty fluorine cell occurs in crystals that are rapidly quenched after hydrogenation. This charge-compensation arrangement is shown in Fig. 1. Both the rare-earth ion and hydride ion possess C_{4v} site symmetry. The local-mode vibrational spectra of these hydride ions give rise to two lines in the infrared absorption spectra of the crystals whose frequencies vary with the particular rare-earth ion present and bear an approximate 2:1 intensity ratio to each other.

The frequencies and widths of these two lines have been reported previously for hydrogenated crystals of calcium fluoride containing cerium.[1] The low-frequency line was assigned as the "longitudinal" (w_z) vibration of the hydride ion and the high-frequency line as the doubly degenerate "trans-

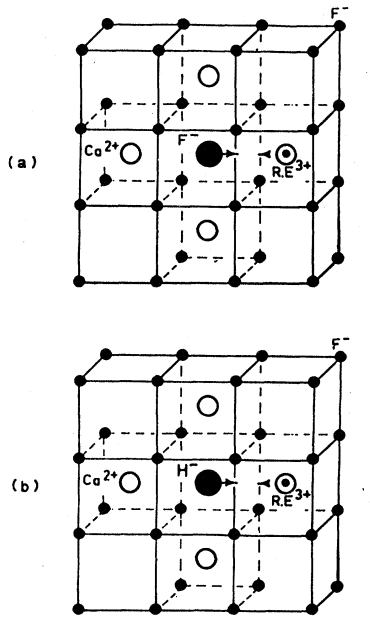

FIG. 1. Schematic representation of the calcium fluoride lattice showing the tetragonal cerium site with (a) charge compensation by interstitial fluoride ions and (b) charge compensation by interstitial hydride ions.

verse" (w_x, w_y) vibration. This assignment was on the basis of the relative intensity of the two lines. However, as pointed out by Newman,[5] the ratios of the intensities are in general significantly different from 2 and an assignment made on this basis could be in error.

In this work, the frequencies, linewidths, and relative intensity of these two lines were determined for hydrogenated and deuterated crystals of calcium and strontium fluoride containing 0.05% cerium; the values are listed in Table I. The measurement of the relative intensity of the lines in the calcium fluoride crystals is rendered more difficult by the occurrence of a broad background absorption near 1130 cm^{-1} due to the lattice phonon band associated with the 965-cm^{-1} tetrahedral hydride site line.

It was not attempted to determine the low-frequency local-mode lines in the crystals containing deuterium or to detect the two lines of the tritium crystals as these lie in a region of strong lattice absorption of the host crystals.

The relative intensities of the two local-mode lines were determined in this work to be 1.0 and 1.3 for hydrogenated crystals of calcium and strontium fluoride containing cerium, respectively. These values are sufficiently different from 2 to be unreliable for determining the assignment of the lines. Furthermore, the anomalous linewidth found previously for the low-frequency line in the hydrogenated calcium fluoride crystal containing cerium was reproduced, and under higher resolution this line resolves into two components separated by 1.3 cm^{-1} (Fig. 2). Similar structure is also found for the corresponding low-frequency line in strontium fluoride where the separation is 1.1 cm^{-1} (Table I). The splitting of the low-frequency local-mode line into two components which maintain their relative intensity down to 4 °K shows that this line is the double-degenerate x, y vibration and not the z vibration as previously assigned. The temperature independence of the relative intensity of the two components rules out the mechanism used by Chambers and Newman[6] to explain the splittings observed in hydrogenated calcium fluoride crystals containing erbium and ytterbium, namely, the presence of an excited electronic level a few cm^{-1} above the ground electronic level.

This new reversed assignment of the localized vibrations is supported by the analysis of the electronic spectrum of the cerium ion presented in Sec. IV E, which shows the high-frequency infrared line to be the z vibration of the hydride ion.

A. Splitting of the x, y Local-Mode Line

The observed splitting of the x, y vibration in the cerium case is attributed to the coupling of the local-mode phonons to the cerium-ion $4f$ electronic states by the electron-phonon interaction, which, in the adiabatic approximation, has the general form[7]

$$V_{ev} = \sum_i f_i^\alpha Q_i^\alpha + \sum_{i,j} g_{ij}^{\alpha\beta} Q_i^\alpha Q_j^\beta + \cdots ,$$

where the f_i^α and $g_{ij}^{\alpha\beta}$ are functions of the electronic coordinates of the cerium $4f$ electron, and the Q_i^α are the phonon normal coordinates, which transform according to the αth irreducible representation of the point group of the cerium-ion site. Because V_{ev} spans the totally symmetric representation of this point group the electronic coordinate functions f_i^α and $g_{ij}^{\alpha\beta}$ form bases for the complex-conjugate representations to these of Q_i^α and $Q_i^\alpha Q_j^\beta$, respectively.

The use of the adiabatic approximation for the formulation of the electron-phonon interaction is justified in this and all subsequent analyses of the cerium-ion spectra by the following:

(a) For the $4f$ electronic levels of the cerium ion, the electron-phonon interaction is small compared to the energy separation between them and to the energies of the hydride-ion local-mode phonons,

(b) For the $5d$ electronic levels of the cerium

TABLE I. Frequencies and linewidths of the infrared absorption lines observed in hydrogenated and deuterated crystals of calcium and strontium fluorides containing 0.05% cerium.

	77 °K			4 °K		
Crystal	Frequency (cm^{-1})	Linewidth (cm^{-1})	Relative intensity	Frequency (cm^{-1})	Linewidth (cm^{-1})	Relative intensity
CaF_2:Ce, H	989.4	1.1	1.0	990.0	0.7	1.0
	990.5	1.1	0.8	991.3	0.7	1.0
	1131.0	8.2	2.6	1131.5	6.5	2.0
CaF_2:Ce, D	817.4	3.7	...	817.8	3.7	...
SrF_2:Ce, H	917.9	2.1	1.0	917.5	0.7	1.0
				918.6	0.7	1.0
	957.3	2.3	0.9	957.7	1.4	1.6
SrF_2:Ce, D	696.3	4.4	...	696.3	4.3	...

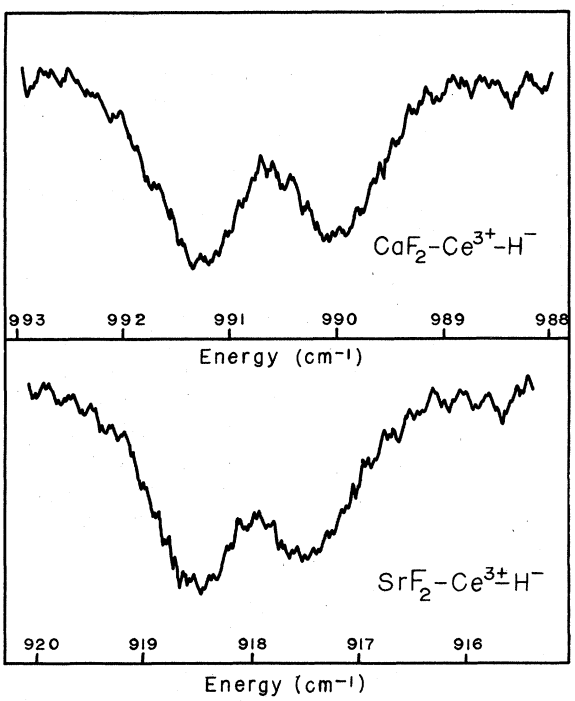

FIG. 2. Recording of the 12 °K infrared spectra of hydrogenated calcium and strontium fluorides containing 0.05% cerium, showing the splitting of the x, y local-mode transition.

ion, the energy separation between them is large compared to the energies of the hydride-ion local-mode phonons so the Born-Oppenheimer approximation is valid.

For the electron-phonon interaction involving the localized modes of the hydrogen, deuterium, or tritium ions alone, the phonon normal coordinates are simply X, Y, and Z, the displacements of these light ions from equilibrium. This follows from the small mass of these ions compared to other atoms of the crystal. For the C_{4v}-site case here, X and Y are degenerate.

To terms quadratic in the phonon coordinates, the electron–local-mode-phonon interaction has the form (for C_{4v} symmetry)

$$V_{ev} = f_x X + f_y Y + f_z Z + (g_{xx} + g_{yy})\tfrac{1}{2}(X^2 + Y^2) + (g_{xx} - g_{yy})\tfrac{1}{2}(X^2 - Y^2) + g_{xy} XY + g_{xz} XZ + g_{yz} YZ + g_{zz} Z^2 ,$$

where the form of the electronic coordinate functions f_i and g_{ij} depends on the particular model used for the electron-phonon interaction.

The simplest model is that of the point charge, where the potential energies of the cerium-ion $4f$ and $5d$ electrons in the electric field of the hydride ion treated as a point charge are evaluated. In the Appendix the form of the f_i and g_{ij} terms are presented for a point-ion model which has the cerium ion located at the origin, the hydride ion at the point (0, 0, D) and the coordinates of the electron of the cerium ion as (x, y, z). The charge of the hydride ion is taken as q located at (X, Y, Z) relative to the equilibrium position of the hydride ion itself. We have $q < 0$ for a negative hydride ion.

Another model of physical significance is the dipole model where the potential energies of the cerium-ion $4f$ and $5d$ electrons in the dipole field of the hydride ion are evaluated. The form of the f_i and g_{ij} terms for this model are also presented in the Appendix while evidence for the hydride-ion dipole moment is presented in Sec. III B.

The splitting of the x, y vibration could occur through the second-degree terms of the electron–local-mode-phonon interaction acting in first-order perturbation on the appropriate vibronic state, which yields terms of the form

$$\langle \varphi(100) | g_{xy} XY | \varphi(010) \rangle ,$$

where φ is the ground-state electronic wave function for the cerium ion. For the C_{4v} site here, the energy-level scheme is as given in Fig. 3, and all $4f$ electronic wave functions of the cerium ion transform as either the γ_6 or γ_7 irreducible representations of the C_{4v} group. The electronic coordinate operator g_{xy} transforms as γ_4 and, since the direct product $\gamma_4 \times \gamma_7 = \gamma_6$, g_{xy} has zero matrix elements between either γ_6 or γ_7 wave functions so the first-order contribution to the x, y splitting vanishes.

Splitting of the x, y vibration can also occur through the first-degree terms $f_x X + f_y Y$ of the electron–local-mode-phonon interaction acting in second-order perturbation. The ground-state wave function for the cerium ion is the $|{}^2F_{5/2}, \Gamma_8, \gamma_7\rangle$ doublet which has the following form when expressed in terms of $|M_L M_S\rangle$ states:

$$\varphi^{\pm} = \sqrt{\tfrac{5}{42}} \left| \mp 2, \mp\tfrac{1}{2} \right\rangle - \sqrt{\tfrac{30}{42}} \left| \mp 3, \pm\tfrac{1}{2} \right\rangle + \sqrt{\tfrac{2}{42}} \left| \pm 1, \pm\tfrac{1}{2} \right\rangle - \sqrt{\tfrac{5}{42}} \left| \pm 2, \mp\tfrac{1}{2} \right\rangle .$$

These Kramers doublet wave functions form a basis for the two rows of the γ_7 irreducible representation of the C_{4v} group.

The x, y splitting is evaluated from the 4×4 interaction matrix formed between the four vibronic states which are linear combinations of product states of the electronic wave functions $\varphi^{\pm}$ and the x, y local-mode-phonon states (100) and (010). The vibronic states transform as the direct product representation $\gamma_7 \times \gamma_5 = \gamma_6 + \gamma_7$. The γ_6 vibronic states are

$$\varphi^{+} \times \tfrac{1}{2}\sqrt{2}\,[(100) + i(010)] , \quad \varphi^{-} \times \tfrac{1}{2}\sqrt{2}\,[(100) - i(010)] , \tag{1}$$

which transform as the spin components $+\frac{1}{2}$ and $-\frac{1}{2}$, respectively. The γ_7 vibronic states are

$$i\varphi^{-} \times \tfrac{1}{2}\sqrt{2}\,[(100) + i(010)] , \quad i\varphi^{+} \times \tfrac{1}{2}\sqrt{2}\,[(100) - i(010)] , \tag{2}$$

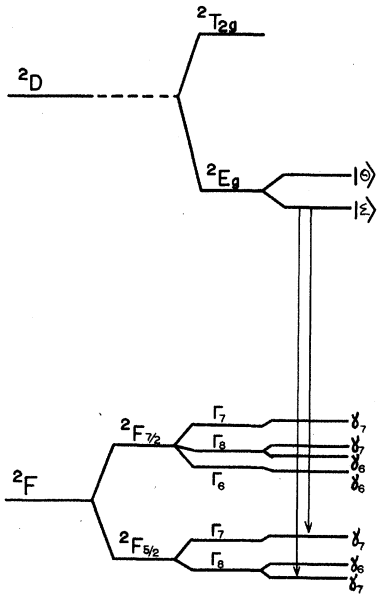

FIG. 3. Electronic energy-level scheme for the cerium ion located in a tetragonal symmetry (C_{4v}) site. The $4f^1$ energy states are labeled by their cubic field and tetragonal field irreducible representations Γ_n and γ_n, respectively. The $5d^1$ energy states are labeled by their cubic field wave functions $|\epsilon\rangle$ and $|\theta\rangle$ defined by (9) and (10). The two fluorescence transitions to the states of the $^2F_{5/2}$ multiplet are shown. The third fluorescence transition observed terminates on one of the states of the $^2F_{7/2}$ multiplet.

which transform in the same way as φ^+ and φ^-, respectively.

The matrix elements of f_xX+f_yY between these vibronic states are evaluated in second-order perturbation theory and are nonzero only for intermediate vibronic states having their electronic wave functions different from either φ^+ or its Kramers conjugate φ^-. The intermediate vibronic states giving a nonzero x, y splitting are those given by the products of the excited electronic states and the (000) and (110) phonon states which are coupled by X and Y operators to (100) and (010), and which transform like the γ_1 and γ_4 irreducible representations, respectively.

The γ_6 wave functions ψ^+ and ψ^- (which transform as spin components $+\frac{1}{2}$ and $-\frac{1}{2}$, respectively) and the (000) and (110) phonon states form intermediate vibronic states which transform as the direct product representations $\gamma_6\times\gamma_1=\gamma_6$ and $\gamma_6\times\gamma_4=\gamma_7$, respectively. The γ_6 intermediate vibronic states are $\psi^+(000)$ and $\psi^-(000)$, which transform like ψ^+ and ψ^-, respectively. The γ_7 intermediate vibronic states are $\psi^-(110)$ and $\psi^+(110)$ which transform like φ^+ and φ^-, respectively.

The γ_7 electronic wave functions θ^+ and θ^- (which transform like φ^+ and φ^-, respectively) and the (000) and (110) phonon states form intermediate vibronic states which transform as the direct product representations $\gamma_7\times\gamma_1=\gamma_7$ and $\gamma_7\times\gamma_4=\gamma_6$, respectively. The γ_7 intermediate vibronic states are $\theta^+(000)$ and $\theta^-(000)$, which transform like φ^+ and φ^-, respectively. The γ_6 intermediate vibronic states are $\theta^-(110)$ and $\theta^+(110)$, which transform like ψ^+ and ψ^-, respectively. Figure 4 gives the vibronic states energy-level scheme.

There are also intermediate vibronic states which are products of the γ_6 and γ_7 electronic states and the $\frac{1}{2}\sqrt{2}\,[(200)\pm(020)]$ phonon states, and which are coupled by the f_xX+f_yY operator to the four vibronic states given by (1) and (2). However, these states result only in a uniform shift in the four vibronic states and produce no net x, y splitting.

The energy shift E_1 of the γ_7 vibronic states (2) produced by the perturbation Hamiltonian f_xX+f_yY acting via the γ_7 intermediate vibronic states defined above is

$$E_1=\frac{\hbar}{2mw_x}\left(\frac{2i\langle\varphi|f_x|\theta\rangle\langle\theta|f_y|\varphi\rangle}{(E_\theta-E_\varphi)-\hbar w_x}-\frac{2i\langle\varphi|f_x|\psi\rangle\langle\psi|f_y|\varphi\rangle}{(E_\psi-E_\varphi)+\hbar w_x}\right). \quad (3)$$

The energy shift E_2 of the γ_6 vibronic states (1) produced by coupling to γ_6 intermediate vibronic states is

$$E_2=\left(\frac{\hbar}{2mw_x}\frac{2i\langle\varphi|f_x|\theta\rangle\langle\theta|f_y|\varphi\rangle}{(E_\theta-E_\varphi)+\hbar w_x}-\frac{2i\langle\varphi|f_x|\psi\rangle\langle\psi|f_y|\varphi\rangle}{(E_\psi-E_\varphi)-\hbar w_x}\right). \quad (4)$$

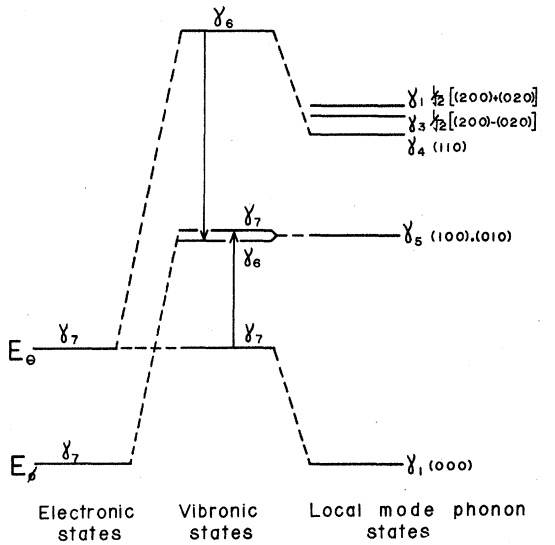

FIG. 4. Vibronic energy-level scheme showing the interactions giving rise to the vibronic splitting of the x, y local-mode vibration for the case of a γ_7 upper electronic state.

E_1 differs from E_2, and the difference constitutes the x, y splitting. This is largest for electronic states whose energy separation from $\varphi^{\pm}$ is comparable to $\hbar w_x$.

For the cerium case here, the electronic states whose energies are close to that of the local-mode phonon $\hbar w_x$ are the $|\,^2F_{5/2},\ \Gamma_7,\ \gamma_7\rangle$ doublet which lies 577 cm^{-1} above the ground state (Sec. IV) and the $|\,^2F_{5/2},\ \Gamma_8,\ \gamma_6\rangle$ doublet whose energy is estimated to be about 200 cm^{-1} above the ground state. These two states of the $^2F_{5/2}$ multiplet have the following wave functions expressed in $|\,M_L M_S\rangle$ states:

$$|\,^2F_{5/2},\ \Gamma_7,\ \gamma_7\rangle = -\sqrt{\tfrac{1}{42}}\,|\mp 2,\ \mp\tfrac{1}{2}\rangle + \sqrt{\tfrac{6}{42}}\,|\mp 3,\ \pm\tfrac{1}{2}\rangle + \sqrt{\tfrac{10}{42}}\,|\pm 1,\ \pm\tfrac{1}{2}\rangle - \sqrt{\tfrac{25}{42}}\,|\pm 2,\ \mp\tfrac{1}{2}\rangle\ , \quad (5)$$

$$|\,^2F_{5/2},\ \Gamma_8,\ \gamma_6\rangle = \sqrt{\tfrac{3}{7}}\,|\,0\mp\tfrac{1}{2}\rangle - \sqrt{\tfrac{4}{7}}\,|\mp 1,\ \pm\tfrac{1}{2}\rangle\ . \quad (6)$$

In the Appendix the electronic coordinate functions f_x and f_y are given in terms of parameters a_{1n} whose value depends on the particular model chosen for the electron-phonon interaction. The matrix elements given in (3) and (4) for the states (5) and (6) are nonzero only for a_{12} and a_{14}:

$$2i\,\langle\,^2F_{5/2},\ \Gamma_8,\ \gamma_7\,|\,f_x\,|\,^2F_{5/2},\ \Gamma_7,\ \gamma_7\rangle \times \langle\,^2F_{5/2},\ \Gamma_7,\ \gamma_7\,|\,f_y\,|\,^2F_{5/2},\ \Gamma_8,\ \gamma_7\rangle = \left[\tfrac{6}{35}\,(\sqrt{10})\langle r^2\rangle\, a_{12}\right]^2 + \left[\tfrac{2}{21}\,(\sqrt{10})\langle r^4\rangle\, a_{14}\right]^2\ ,$$

$$2i\,\langle\,^2F_{5/2},\ \Gamma_8,\ \gamma_7\,|\,f_x\,|\,^2F_{5/2},\ \Gamma_8,\ \gamma_6\rangle \times \langle\,^2F_{5/2},\ \Gamma_8,\ \gamma_6\,|\,f_y\,|\,^2F_{5/2},\ \Gamma_8,\ \gamma_7\rangle = \left[\tfrac{2}{35}(\sqrt{6})\langle r^2\rangle\, a_{12}\right]^2 + \left[\tfrac{5}{63}(\sqrt{6})\langle r^4\rangle\, a_{14}\right]^2\ .$$

Using these values for the matrix elements together with the point-charge model values for a_{12} and a_{14} of eq/D^4 and eq/D^6 yields the contribution of the $|\,^2F_{5/2},\ \Gamma_7,\ \gamma_7\rangle$ and $|\,^2F_{5/2},\ \Gamma_8,\ \gamma_6\rangle$ states to the x, y splitting as 5.2 and -0.2 cm^{-1}, respectively. The net x, y splitting of 5.0 cm^{-1} is in reasonable agreement with the experimentally observed value especially when the approximations inherent in the point-charge model are considered.

Other $4f$ electronic states of the cerium ion also contribute, but to a lesser extent. The four wave functions $|\,^2F_{7/2},\ \Gamma_7,\ \gamma_7\rangle$, $|\,^2F_{7/2},\ \Gamma_8,\ \gamma_7\rangle$, $|\,^2F_{7/2},\ \Gamma_8,\ \gamma_6\rangle$, and $|\,^2F_{7/2},\ \Gamma_6,\ \gamma_6\rangle$ of the $^2F_{7/2}$ multiplet have energies at least 2000 cm^{-1} above the ground state. Their $|\,M_L M_S\rangle$ form is given by Bessent and Hayes[8] and the net total contribution of all four wave functions to the x, y splitting is 0.1 cm^{-1}. The total net x, y splitting from all $4f^1$ configuration states is 5.1 cm^{-1}.

For the dipole model, a_{12} and a_{14} have the values $5ep/D^5$ and $7ep/D^7$, respectively, and with $p/e = 1.1$ Bohr radii (Sec. III B) there is a further contribution to the x, y splitting from all $4f^1$ configuration states of 6.4 cm^{-1}.

The x, y splitting for strontium fluoride can be calculated in a similar way and is expected to be comparable as the electronic states are the same and only their energy separations relative to the somewhat different local-mode frequencies will be altered.

Other mechanisms yielding a possible x, y splitting are the second-degree electron-phonon interaction terms acting in second-order perturbation by intermediate electronic states, as for the first-degree terms above, or via intermediate phonon states involving the z local-mode vibration. Both these mechanisms give values that are too small to account for the observed splitting, as can be expected.

The experimental x, y splitting observed here for cerium is small, being comparable to the width of the local-mode lines themselves and is only apparent in the 4 °K spectra (Fig. 2). Praseodymium also shows an x, y splitting of 3 cm^{-1}, at 4 °K, which is due to a somewhat different mechanism to that described here for cerium, and this will be discussed elsewhere. Similar x, y splittings have not yet been reported for any other rare-earth ions. However, these may show small splittings if examined under a higher resolution than 0.5 cm^{-1} and with crystal temperatures below 10 °K.

B. Interaction between Adjacent Rare-Earth and Hydride-Ions

The frequency separation between the two infrared lines of the C_{4v} site was taken in previous work[1] as due to the perturbing effect of the extra electric charge of the adjacent rare-earth ion on the triply degenerate transition of an isolated interstitial hydride ion. It was shown that for a purely electrostatic model the frequency of the z vibration would be lower than that of the x, y vibration. It is now necessary to reexamine this model in view of the new assignment for the local-mode vibrations. It is possible to explain the infrared observations in the following way.

The electric field of an extra electric charge on the rare-earth ion results in a nonlinear polarization of the hydride ion, and the ground state of the hydride ion is no longer a pure $1s^2$ configuration, but has an admixture of the $1s2p$ configuration present. This seems to be confirmed by a measurement of the transferred hyperfine splitting of the ground state of the cerium ion,[9] which exhibits a large anisotropy. This polarization of the hydride ion can be conveniently represented by a dipole moment directed towards the rare-earth ion. This dipole moment is assumed to have a constant magnitude, independent of the instantaneous position of the hydride ion.

The hydride ion moves in a potential well whose potential may be expanded as a power series in the

hydride-ion displacements:

$$V = a(X^2+Y^2) + bZ^2 + cZ^3 + dZ(X^2+Y^2) + f(X^4+Y^4) + gZ^4 + hZ^2(X^2+Y^2) + kX^2Y^2 .$$

This field can be considered as a combination of the undeformed cubic potential of the isolated interstitial hydride-ion site and the electrostatic attraction of an extra positive charge in the adjacent cube. The hydride ion interacts with this field both through its point charge q and its dipole moment p, and for these interactions the harmonic and cubic anharmonic constants a, b, c, and d have the form

$$a = A + \frac{1}{2}\frac{\sigma q}{D^3} + \frac{p\sigma}{D^4} - \frac{2Ap}{qD} ,$$

$$b = A - \frac{\sigma q}{D^3} - \frac{3p\sigma}{D^4} ,$$

$$c = \frac{\sigma q}{D^4} + \frac{4p\sigma}{D^5} , \tag{7}$$

$$d = -\frac{3\sigma q}{2D^4} - \frac{4p\sigma}{D^5} + \frac{3Ap}{qD^2} . \tag{8}$$

Here D is the distance between the rare-earth ion and the equilibrium position of the hydride ion, σ and q are the effective extra charge of the rare-earth ion and the hydride ion, respectively, and A is the constant of the harmonic potential energy for the isolated interstitial hydride ion.

The observed frequencies of the local modes of the hydride ion in the cubic interstitial site and in the C_{4v} site are approximately their harmonic values:

$$w_c = (2A/m)^{1/2} , \quad w_{x,y} = (2a/m)^{1/2} , \quad w_z = (2b/m)^{1/2} ,$$

where m is the hydride-ion mass.

The effect of the hydride-ion dipole moment p is to lower the frequency of the x, y vibration so both the z and x, y frequencies can be less than the cubic-site frequency, as observed, for a sufficiently large value of p. The ionic radius of the calcium ion is approximately in the middle of the range of rare-earth-ion radii so the distortion of the lattice caused by replacement of a calcium ion by a rare-earth ion should be least for these ions. The gadolinium frequency values were, therefore, taken as representative for the calculation of the value of p. For $q = \sigma = 0.85e$, the value of p/q is calculated to be 1.3 Bohr radii, so $p/e = 1.1$ Bohr radii. These values of p, q, and σ will be taken in all the following numerical calculations.

These values are large for a hydrogen atom having a charge of one proton, but are not unreasonably so. The hydride-ion polarizability has been measured[10] for small electric fields and corresponds to a value of $p/e = 7.7$ Bohr radii. The value of p/e will be less than this at high fields, because of the nonlinear dependence of the polarizability on field; the value of 1.1 Bohr radii obtained above from the infrared spectra corresponds to the saturation value of the hydride-ion dipole moment.

The dipole moment p of the hydride ion can explain qualitatively the deviation of the relative intensity of the two local-mode lines from about 2. The intensity of a given local-mode line is proportional to the square of the matrix element of the electric dipole operator between the corresponding harmonic oscillator ground and excited states. For the x, y vibration of the hydride ion, rotation of the dipole moment about the Z axis occurs. This interacts with the electric field of the incident radiation to yield a net intensity for the x, y vibration line of $2(q - p/D)^2\hbar/2mw_x$, whereas the intensity for the z vibration line is $\hbar q^2/2mw_z$. The intensity of the x, y vibration is, therefore, reduced by a factor of $(1 - p/qD)^2$ relative to the z vibration. For $p/e = 1.1$ Bohr radii, this factor is 0.56 and the net relative intensity of the two lines is 1.3 with the x, y vibration the more intense, in good agreement with the observed value of 1.0 for calcium fluoride crystals containing cerium. For strontium fluoride, the corresponding calculation yields 1.2, as compared to the experimental ratio of 1.3.

IV. ULTRAVIOLET ABSORPTION AND FLUORESCENCE SPECTRA

Trivalent cerium has a relatively simple electronic energy level scheme[11] (Fig. 3). Transitions between the $^2F_{5/2}$ and $^2F_{7/2}$ multiplets of the $4f^7$ configuration occur in the 2000-cm^{-1} infrared region while the first $4f \rightarrow 5d$ transition appears in the ultraviolet around 3000 Å. The absorption spectra observed in the ultraviolet are characteristic of electronic transitions coupling fairly strongly with vibrations of the host lattice. The spectra possess sharp zero-phonon electronic lines with broad vibronic sidebands which show vibrational structure at low temperatures. Such spectra are characteristic of d electronic states rather than well-shielded f electronic states.

A. Ultraviolet Spectra of Parent Crystals

The low-temperature ultraviolet absorption spectra of calcium fluoride crystals containing 0.05% cerium show several sharp absorption lines in the 3000–3200-Å region due to $4f$-$5d$ transitions of cerium whose positions differ for the different crystal fields associated with the various possible site positions and charge-compensation arrangements for the cerium ion in the calcium fluoride lattice.[12] The strongest of these absorption lines in 0.05%-concentration crystals is the well-characterized line at 3131.9 Å, which arises from cerium ions in a site of tetragonal (C_{4v}) symmetry where charge compensation of the cerium ion is achieved by a

fluoride ion situated in an adjacent empty cell. Figure 1 shows this charge-compensation arrangement. The analogous lines in strontium and barium fluoride crystals containing cerium are at 3014 and 2965 Å, respectively.

Associated with these electronic lines are vibronic sidebands which are resolved at low temperatures into a number of peaks (Fig. 5). These have been shown by Kapalanskii *et al.*[3] to comprise the lattice frequency spectra of the host crystals superposed on a vibrational progression whose frequency was reported as 485, 445, and 405 cm^{-1} for calcium, strontium, and barium fluoride crystals, respectively. These vibrational frequencies were redetermined in this work to be 484 ± 1, 438 ± 1, and 403 ± 1 cm^{-1}, respectively, in good agreement with the results of Kapalanskii *et al.*

In the fluorescence spectra of the parent crystals, Kapalanskii *et al.* observed transitions from the lowest level of the $5d$ configuration to two crystal-field levels of the $^2F_{5/2}$ and $^2F_{7/2}$ multiplets of the $4f^1$ configuration. Each of these transitions has an associated vibronic sideband comprising the lattice frequencies of the host crystal superposed on a vibrational progression whose repetition frequency was reported as 475, 425, and 415 cm^{-1} for calcium, strontium, and barium fluorides, respectively. In the measurements done here, disagreement was found with the barium fluoride value and the revised values obtained for all three fluorides are 478 ± 1, 424 ± 1, and 398 ± 1 cm^{-1}, respectively. In all cases the vibrational progression frequencies observed in absorption are slightly larger than those observed in fluorescence and the apparent anomaly shown by barium fluoride in the earlier measurements of Kapalanskii *et al.* does not appear.

B. Ultraviolet Spectra of Hydrogenic Sites

When a hydride ion occupies a site near a cerium ion, the energy levels of the latter are perturbed by the change in the environment and new lines appear. Since, in general, the number of cerium ions and their valency do not change during the hydrogenation process, the new hydrogenic sites grow at the expense of the existing sites.

After hydrogenation, the absorption spectra of the crystals show new electronic lines whose frequencies are listed in Table II. The deuterated and tritiated crystals show analogous lines whose frequencies are slightly shifted from those of the hydrogenated crystals. Crystals heated in a mixed

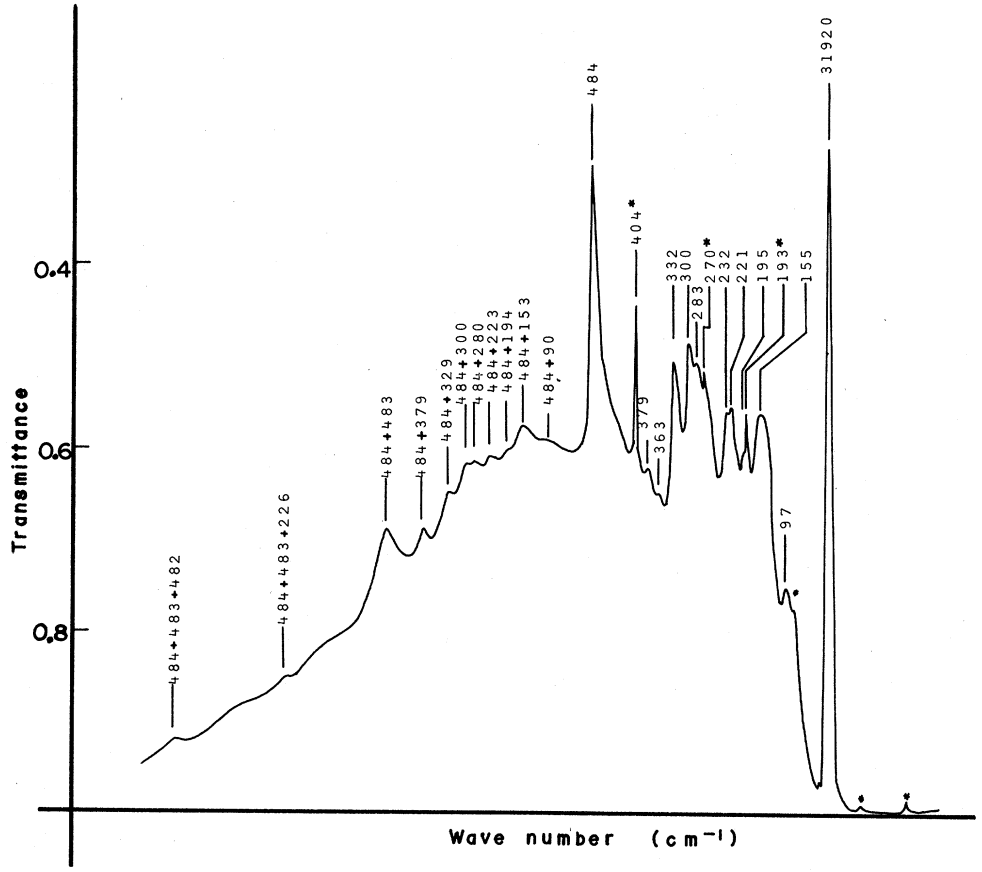

FIG. 5. Ultraviolet absorption spectrum of crystals of calcium fluoride containing 0.05% cerium recorded at 12 °K. The separations of the peaks in the vibronic spectrum from the no-phonon electronic transition at 3131.9 Å are shown in cm^{-1}; the lines marked with asterisks are electronic transitions.

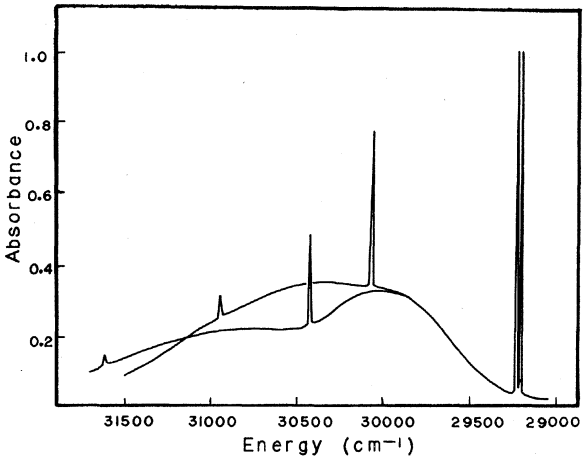

FIG. 6. Ultraviolet absorption spectra of hydrogenated and deuterated crystals of calcium fluoride containing 0.05% cerium recorded at 12 °K. The lattice phonon structure has been smoothed out to show the underlying broad absorption envelope.

hydrogen-deuterium atmosphere display both lines. These isotope shifts show that the new lines are associated with cerium sites involving a single hydrogen, deuterium, or tritium ion.

The lines at 3417.9, 3420.7, and 3421.9 Å for the hydrogenated, deuterated, and tritiated calcium fluoride crystals, respectively, are at least a factor of 40 stronger than the others and occur at sufficient intensity to show well-developed vibronic sidebands in both absorption and fluorescence. Similar vibronic sidebands are observed associated with the analogous 3244.8-, 3248.3-, and 3250.0-Å lines present in hydrogenated, deuterated, and tritiated strontium fluoride crystals, respectively. In the case of barium fluoride a hydrogenic-site absorption band appears which has no structure down to 2 °K, while for calcium and strontium fluorides, the structure becomes apparent below 150 and 80 °K, respectively. The infrared local-mode spectrum for barium fluoride showed that the tetragonal hydrogenic-site lines do not appear so the optical band observed must be due to another hydrogenic site.

The general features of the absorption spectra are shown in Figs. 6 and 7 for calcium and strontium fluorides, respectively. At low temperatures there is a broad and intense absorption band on the high-energy side of the zero-phonon electronic lines. Superposed on this band are sharp vibronic lines corresponding to the z local modes of hydrogen, deuterium, or tritium. These lines are relatively strong and it is possible to detect, in addition, vibronic lines corresponding to second harmonic local modes of hydrogen and deuterium (see Table III). The vibronic lines thus form the first two members of a local-mode vibrational series. Onset of intense absorption at shorter wavelengths due to the normal fluoride-ion charge-compensated cerium ion in the tetragonal site prevents observation of additional higher and weaker members of this series.

Associated with each of these local-mode vibronic lines as well as with the zero-phonon electronic lines are weaker vibronic lines whose frequency separation from their parent lines can be matched to those of the lattice spectrum of the host fluoride crystals. The observed frequencies are listed in Tables IV and V and their assignment is discussed in Sec. VII.

Investigations of the shape of the broad and intense absorption band show that it can be resolved into broad overlapping envelopes associated with the zero-phonon electronic lines and with the local-mode vibronic lines and the apparent difference in the band shape between the hydrogenic and deuterium spectra is simply a consequence of the greater separation of the local-mode vibronic lines from the corresponding zero-phonon electronic line in the hydrogen case (Figs. 6 and 7). In the parent fluoride crystals, the band is significantly different from the hydrogen and deuterium ones in being centered closer to its associated electronic line (Fig. 5).

The fluorescence spectra of the hydrogenic sites

TABLE II. Electronic lines appearing in the ultraviolet absorption spectra of hydrogenated, deuterated, and tritiated crystals of calcium and strontium fluoride containing 0.05% cerium. Temperature of the crystals 12 °K.

Crystal	Wavelength of line in hydrogenated crystal (Å)	Wavelength of line in deuterated crystal (Å)	Wavelength of line in tritiated crystal (Å)	Isotope shifts: Hydrogen to deuterium	Isotope shifts: Hydrogen to tritium
	3417.7	3420.5	3421.9	23.8	35.1
CaF_2: Ce^{3+}	3369.6	3371.6	3372.4	17	25
	3355.6	3355.1	...		
	3357.2	3356.6	...	−4.8	...
SrF_2: Ce^{3+}	3244.8	3248.3	3249.9	33.4	49.1

are relatively weak. However, at both 77 and 4 °K it is possible to observe vibronic lines whose frequency separation from their respective electronic lines match the hydride and deuteride local-mode frequencies observed in the infrared. Table VI shows the frequency correlation. The parent zero-phonon electronic lines are, therefore, identified as the hydride, deuteride, and tritide analogs of the fluoride-ion charge-compensation site observed in the parent crystals with the site arrangement given in Fig. 1. The occurrence of such hydrogenic sites has been confirmed in the ENDOR measurements by Baker *et al.*[13]

As in the case of absorption, the fluorescence spectrum does not show the vibronic lines arising from the other member of the pair of infrared local-mode lines because this vibronic transition is forbidden (Sec. IV E). Other fluorescence lines observed arise from transitions to crystal field levels of the $^2F_{5/2}$ and $^2F_{7/2}$ multiplets and to local-mode vibronic levels associated with these levels (Table VI).

In the absorption spectra of the hydrogenated, deuterated, and tritiated calcium fluoride crystals, other hydrogenic lines are present (Table II), but these do not bear a constant intensity ratio either to the principal hydrogenic-site line or among themselves, so they must arise from other hydrogenic sites in the crystal. Of these lines, an interesting doublet at 3355.6 and 3357.2 Å occurs at typically $\frac{1}{50}$ of the intensity of the principal hydrogenic site

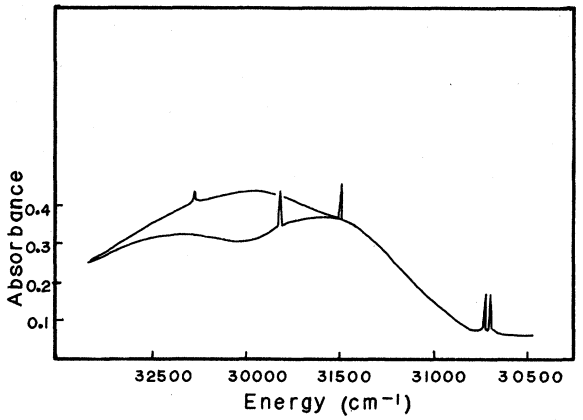

FIG. 7. Ultraviolet absorption spectra of hydrogenated and deuterated crystals of strontium fluoride containing 0.05% cerium recorded at 12 °K. The lattice phonon structure has been smoothed out to show the underlying broad absorption envelope.

TABLE III. Electronic and local-mode vibronic lines of hydrogen, deuterium, and tritium sites in calcium and strontium fluoride crystals containing 0.05% cerium. Crystal temperature 12 °K.

Crystal	Wavelength of line (Å)	Assignment	Separation from parent line (cm^{-1})	Relative intensity	Linewidth (cm^{-1})
$CaF_2:Ce^{3+}, H^-$	3417.7	Parent electronic line	···	1	5.1
	3279.3	First H^- local-mode vibronic	1235	0.54	10.2
	3155.1	Second H^- local-mode vibronic	2435	0.07	12.9
$CaF_2:Ce^{3+}, D^-$	3420.5	Parent electronic line	···	1	5.2
	3319.1	First D^- local-mode vibronic	893	0.61	7.5
	3225.4	Second D^- local-mode vibronic	1768	0.13	11.5
$CaF_2:Ce^{3+}, T^-$	3421.9	Parent electronic line	···	1	5.8
	3337.4	First T^- local-mode vibronic	739	0.70	9.4
$SrF_2:Ce^{3+}, H^-$	3244.8	Parent electronic line	···	1	6.4
	3132.7	First H^- local-mode vibronic	1103	1.05	7.9
$SrF_2:Ce^{3+}, D^-$	3248.3	Parent electronic line	···	1	6.2
	3165.8	First D^- local-mode vibronic	802	1.10	7.0
	3089.6	Second D^- local-mode vibronic	1581	0.39	9.9
$SrF_2:Ce^{3+}, T^-$	3249.9	Parent electronic line	···	1	6.2
	3180.8	First T^- local-mode vibronic	669	0.6	9

line at 3417 Å. The line at 3370 Å also has a typical intensity of $\frac{1}{50}$ relative to the 3417-Å line. By suitable treatment of the crystals, the intensity of the doublet can be enhanced sufficiently for the related hydrogen and deuterium local-mode vibronics to become apparent and these are displaced 1235 and 890 cm^{-1}, respectively, from the parent lines, i.e., at the same frequency separation as observed for the principal tetragonal symmetry hydrogenic and deuterium sites. This result indicates that the doublet arises from the same cerium charge-compensating interstitial hydride-ion pair situated in a different lattice configuration.

C. Absorption and Fluorescence Spectra of the Hydrogenated, Deuterated, and Tritiated Crystals after Ultraviolet Irradiation

Irradiation by the unfiltered output from a high-pressure mercury lamp causes the spectra of the principal hydrogenic sites to decrease in intensity and new spectra appear at longer wavelengths. This conversion is only partially effective above 77 °K, and the new spectra rapidly reconvert to the original on warming to higher temperatures. The conversion does not occur at 4 °K which indicates that it involves the rearrangement of atoms. The spectra of the new sites are similar to those of the original sites and consist of sharp zero-phonon electronic lines with associated vibronic sidebands possessing vibrational fine structure (Table VII). Only one local-mode vibronic of the light ion appears together with the vibrational progression frequency characteristic of the fluoride-ion site of the parent crystal. From this it can be deduced that this new irradiation site involves both hydride and fluoride interstitial ions, but the site arrangement of these is unknown. This new irradiation site thus does not correspond to the neutral hydrogen atom site found for gadolinium[1] but appears to have analogies with a second irradiation site found for gadolinium[14] whose electronic line is at 3118 Å, the hydrogen vibronic interval is 1416 cm^{-1}, and the deuterium vibronic interval is 1026 cm^{-1}.

In the calcium fluoride crystals which possess in addition the doublet near 3356 Å there appears after irradiation a new doublet at longer wavelengths. The frequencies of the lines of this doublet are also listed in Table VII.

Electron-spin-resonance investigations would be useful for determining the site arrangements for these irradiation sites.

TABLE IV. Vibrational sidebands associated with the (i) 3417.7-Å electronic line observed in hydrogenated crystals, (ii) the first local-mode vibronic line observed in hydrogenated crystals, (iii) the 3420.5-Å electronic line observed in deuterated crystals, (iv) the first local-mode vibronic line of deuterium observed in deuterated crystals, and (v) the second local-mode vibronic line of deuterium observed in deuterated crystals. All values are in cm^{-1} and are accurate to ±3 cm^{-1}. The crystals were calcium fluoride containing 0.05% cerium and the spectra were recorded at 12 °K. The parent line for the vibronics is at the head of each column.

3417.7 Å	3279.3 Å	3420.5 Å	3319.1 Å	3225.4 Å
107 ± 8	100	100	100	···
170*	169	168	170	···
182	181	182	183	185
192	191	193	193	
238	237	237	237	235
284	280	283	279	280
319	320	318	319	320
330	333	332	330	···
368	367	368	367	···
435	433	433	435	430
475	472	474	476	···
512	510	513	511	···
564	554	563	553	···
612	614	615	610	···
650	···	655	650	···
700	···	701	700	···
746	748	750	743	

TABLE V. Vibrational sidebands associated with the (i) 3244.8-Å electronic line observed in hydrogenated crystals, (ii) the first local-mode vibronic line observed in hydrogenated crystals, (iii) the 3248.3-Å electronic line observed in deuterated crystals, and (iv) the first local-mode vibronic line observed in deuterated crystals. All values are in cm^{-1} and are accurate to ±3 cm^{-1} and are accurate to ±3 cm^{-1}. The crystals were strontium fluoride containing 0.05% cerium and the spectra were recorded at 12 °K. The parent line for the vibronics is at the head of each column.

3244.8 Å	3132.7 Å	3248.3 Å	3165.8 Å
121	120	120	119
171	171	170	168
180	···	180	···
196	197	197	195
240	241	244	243
272	270	272	270
291	289	292	289
320	322	321	319
400	394	399	396
···	520[a]	···	···
535	540	540	535
···	560[a]	···	···
674	669	674	671
800	790	···	···

[a] Just resolved lines.

D. Analysis of Electronic Spectra

The principal zero-phonon electronic line present in the ultraviolet absorption spectra of the parent, hydrogenated, deuterated, and tritiated crystals arises from cerium ions located in the tetragonal symmetry C_{4v} site shown in Fig. 1. The electronic transition is from the lowest level

of the $4f^1$ configuration to the lowest level of the $5d$ configuration and is electric dipole allowed.

The effect of the tetragonal symmetry field on the d levels of cerium is described by Starostin.[11] The ^2D free-ion multiplet is split by the cubic component of the crystal field into an orbital triplet $^2T_{2g}$ and an orbital doublet ^2E_g with the latter lowest, and these are further split by the noncubic component. It is generally accepted that the $^2T_{2g}$ levels lie in the 2000-Å region, and Kapalanskii *et al.* identified the over-all splitting of the $^2T_{2g}$ and E_g levels as 8810 cm^{-1} for the tetragonal cerium site in the parent calcium fluoride crystal. Loh[15] has postulated a large tetragonal splitting of the E_g level placing one of these at 2020 Å just below the T_{2g} group, while the other is the 3131.9-Å line. However, it is more reasonable to suppose that the second component of the E_g level lies in the 3000-Å region, and that its nonobservation is due either to its low spectral intensity or to its being a broad line.

A careful search was made for this second component of the E_g level in the hydrogenated and deuterated calcium fluoride crystals, but no evidence of it was found. All the other electronic lines reported in Table II do not show the necessary intensity correlation with the main zero-phonon electronic line to be assigned as this second component. Its nonobservation sets an upper limit on its possible intensity. If its width is taken to be the same as the main zero-phonon line at 3417 Å this upper limit is $\frac{1}{200}$ of that line's intensity.

The cubic field wave functions $|\epsilon\rangle$ and $|\theta\rangle$ appropriate for the two $5d^1$ configuration E_g levels have the following form expressed in terms of $|M_L, M_S\rangle$ states:

$$|\epsilon\rangle = \tfrac{1}{2}\sqrt{2}\,|\pm 2, \pm\tfrac{1}{2}\rangle + \tfrac{1}{2}\sqrt{2}\,|\mp 2, \pm\tfrac{1}{2}\rangle\,, \tag{9}$$

$$|\theta\rangle = |0, \pm\tfrac{1}{2}\rangle\,, \tag{10}$$

while the wave function for the lowest level $|^2F_{5/2}, \Gamma_8, \gamma_7\rangle$ of the $4f^1$ configuration has already been given in Sec. III A. The relative intensity of the two $4f \rightarrow 5d$ transitions can be calculated using these wave functions, and the net intensity ratio of the two transitions for incident unpolarized light is $\frac{3}{49}$. The nonobservation of the second component of the E_g level is consistent with this result.

The shift of the electronic lines of the hydrogen, deuterium, and tritium sites from those of the parent site must be a consequence of the substitution of a hydride, deuteride, or tritide ion for the fluoride-ion charge compensating the trivalent cerium ion. Such a substitution can affect the energy levels of the cerium ion either through a change in the crystal field splitting or through a change in the center of gravity of the ^2D multiplet of the cerium ion. It has been shown by Manthey[16] that crystal of calcium fluoride containing cerium frequently show additional lines in the 3090-Å region of which the line at 3092.2 Å can be attributed to trivalent cerium ions located in cubic sites. The lines of the parent- and hydride-ion tetragonal sites are displaced 410 and 3080 cm^{-1}, respectively, from this cubic-site line and this difference cannot be explained solely by a change in the crystal field splitting of the ^2D multiplet. The ^2D multiplet is centered at lower energies for the hydrogenic site, and either is a consequence of a reduced central field acting on the cerium ion in the hydrogenic site through covalency and overlap effects,

TABLE VI. Fluorescence spectra data for hydrogenated, deuterated, and tritiated crystals of calcium and strontium fluorides containing 0.05% cerium showing the correlation of the local-mode vibronics observed in fluorescence with the local-mode frequencies observed directly in the infrared. Crystal temperature 12 °K.

Crystal	Terminating state of the transition	Wavelength of electronic line (Å)	Wavelength of the vibronic line (Å)	Separation (cm^{-1})	Infrared-mode frequency (cm^{-1})
$CaF_2:Ce^{3+}, H^-$	$^2F_{5/2}\,\|\,\Gamma_8, \gamma_7\rangle$ ground state	3417.7	3554.7	1131±4	
$CaF_2:Ce^{3+}, H^-$	$^2F_{5/2}\,\|\,\Gamma_7, \gamma_7\rangle$	3486.6	3628.1	1120	1131
$CaF_2:Ce^{3+}, H^-$	$^2F_{7/2}$	3691.8	3853.4	1135	
$CaF_2:Ce^{3+}, D^-$	$^2F_{5/2}\,\|\,\Gamma_8, \gamma_7\rangle$	3420.5	3517.7	816±4	
$CaF_2:Ce^{3+}, D^-$	$^2F_{5/2}\,\|\,\Gamma_7, \gamma_7\rangle$	3489.4	3590.7	806	817
$CaF_2:Ce^{3+}, D^-$	$^2F_{7/2}$	3695.1	3810.3	818	
$CaF_2:Ce^{3+}, T^-$	$^2F_{5/2}\,\|\,\Gamma_8, \gamma_7\rangle$	3421.9	3503.5	672	
$CaF_2:Ce^{3+}, T^-$	$^2F_{5/2}\,\|\,\Gamma_7, \gamma_7\rangle$	3490.8		...	
$CaF_2:Ce^{3+}, T^-$	$^2F_{7/2}$	3696.5			
$SrF_2:Ce^{3+}, H^-$	$^2F_{5/2}\,\|\,\Gamma_8, \gamma_7\rangle$	3244.8	...	...	
$SrF_2:Ce^{3+}, D^-$	$^2F_{5/2}\,\|\,\Gamma_8, \gamma_7\rangle$	3248.3	3323.5	696	
$SrF_2:Ce^{3+}, T^-$	$^2F_{5/2}\,\|\,\Gamma_8, \gamma_7\rangle$	3250.0	...	...	

or is due to the configurational interactions of the crystal field depressing the ^2D multiplet to lower energies in the hydrogenic site. No attempt has been made to make quantitative calculations for these two possible effects.

There are three crystal field levels arising from the $^2F_{5/2}$ multiplet and four from the $^2F_{7/2}$ multiplet of the $4f^1$ configuration and fluorescence transitions have been observed to two levels of the $^2F_{5/2}$ multiplet and to one of the levels of the $^2F_{7/2}$ multiplet (Table VI). Comparison of these data for the hydrogenic site with that of the fluoride-ion site shows that there is little difference in either crystal field or spin-orbit coupling between the two sites. The separation of the two fluorescence transitions to the $|^2F_{5/2}, \Gamma_8, \gamma_7\rangle$ and $^2F_{7/2}$ levels are 2171 and 2189 cm^{-1} for the hydrogenic- and fluoride-ion site, respectively, while the $|^2F_{5/2}, \Gamma_7, \gamma_7\rangle$ level is located 577 and 578 cm^{-1}, respectively, above the corresponding $|^2F_{5/2}, \Gamma_8, \gamma_7\rangle$ ground state for these same two sites.

The nonobservation of the remaining expected fluorescence transitions is a consequence of the smaller transition probabilities for these transitions, coupled with the effect of nonradiative processes.

E. Origin of Vibronic Transitions

A characteristic feature of all the cerium spectra is the appearance of only one local-mode vibronic line progression in either the absorption or the fluorescence spectra whereas two local-mode lines are observed in infrared absorption. The intensity and width of these local-mode vibronic lines are comparable to those of the parent electronic lines. For the $4f^n \rightarrow 4f^n$ systems previously studied[1] both local-mode lines appear in the vibronic spectra.

The observed vibronic transitions arise from the coupling of the cerium ion's electronic states to the lattice and local-mode phonons by the electron-phonon interaction whose form has already been presented in Sec. III. The different form of the f_z from the f_x and f_y functions results in the appearance of only a local-mode vibronic transition corresponding to the z vibration of the hydride ion whereas the corresponding x and y vibronic transitions are absent. The derivation proceeds as follows:

Following Bron,[17] the total wave function $\Psi_{in}(r, Q)$ for the coupled electron-phonon system can be written, in the Born-Oppenheimer approximation, as a product of an electronic wave function $\varphi_i(r, Q)$ and a nuclear wave function $\psi_{in}(Q)$:

$$\Psi_{in}(r, Q) = \varphi_i(r, Q)\,\psi_{in}(Q) ,$$

where r represents the electron coordinates and Q the nuclear coordinates.

The probability of an electric dipole transition between these electron-phonon states is

$$\langle \Psi_{in}(r, Q)|\, P\,|\, \Psi_{jn'}(r, Q)\rangle = \langle \varphi_i(r, Q)|\, P\,|\, \varphi_j(r, Q)\rangle \times \prod_k \langle \psi_{in}(Q^{(k)} - \alpha_{0i}^{(k)})|\, \psi_{jn'}(Q^{(k)} - \alpha_{0j}^{(k)})\rangle ,$$

where P is the electric dipole operator, φ_j is the electronic wave function for the jth electronic state, ψ_{jn} is the corresponding nuclear wave function in the jth electronic state and nth nuclear state, and $\alpha_{0j}^{(k)}$ is the shift in the equilibrium position for the jth electronic state. The $\alpha_{0j}^{(k)}$ are given by

$$\alpha_{0j}^{(k)} = \frac{1}{m w_k^2} \langle \varphi_j |\, f_k\,|\, \varphi_j \rangle ,$$

where w_k is the frequency of the kth normal mode. The appearance of vibronics is determined by the nonvanishing of the displacement parameter $(\alpha_{0i}^{(k)} - \alpha_{0j}^{(k)}) = \alpha_0^{(k)}$ between the ground and excited electronic states, φ_i and φ_j.

The first nonvanishing matrix element of f_k involves the constant term T_0^0 in f_z and this gives a

TABLE VII. Electronic and local-mode vibronic lines of hydrogen, deuterium, and tritium irradiation sites in calcium and strontium fluoride crystals containing 0.05% cerium. Crystal temperature 12 °K.

Crystal	Wavelength of line in hydrogenated crystal (Å)	Wavelength of line in deuterated crystal (Å)	Wavelength of line in tritiated crystal (Å)	Isotope shift: Hydrogen to deuterium (cm^{-1})	Isotope shift: Hydrogen to tritium (cm^{-1})
CaF_2:Ce	3548.9	3547.1	3546.3	−14.2	−20.6
	3458.5	3457.3	...	−10	...
	3459.7	3458.5	...	−10	...
SrF_2:Ce	3391.0	3389.5	3388.4	−13.4	−20.0

Crystal	CaF_2:Ce, H	CaF_2:Ce, D	CaF_2:Ce, T	SrF_2:Ce, D
Wavelength of vibronic line (Å)	3367.1	3424.5	3345.5	3285.0
Vibrational interval (cm^{-1})	1421	1009	825	940

net shift $\alpha_0^{(Z)}$ only if the value of this matrix element differs for a $4f$ and a $5d$ electronic state. This is not the case, since the effect of a constant term is to shift all energy levels of the cerium ion equally with no net difference between levels. The next nonvanishing matrix elements are those involving the quadratic terms in f_x, f_y, and f_z and for these the difference in their contribution for $4f$ and $5d$ electronic states immediately follows from the difference in $\langle r^n \rangle$ for these states. The wave functions appropriate for the $4f \rightarrow 5d$ transition observed here have been given in Sec. III and using these together with the values of $\langle r^2 \rangle_{4f}$, $\langle r^4 \rangle_{4f}$, and $\langle r^2 \rangle_{5d}$ given by Bron and $\langle r^4 \rangle_{5d} = 70.66$ a.u. extrapolated from the data of Rajnak[18] gives the point-charge model contribution to the $\alpha_0^{(Z)}$ shift as 0.07 Å and the dipole model contribution as 0.07 Å. The corresponding quadratic terms of f_x and f_y do not contribute in first order for the particular upper d electronic state observed here so the $\alpha_0^{(X)}$ and $\alpha_0^{(Y)}$ shifts are zero.

Local-mode vibronics involving the Z vibration of the hydride ion are thus the only ones expected to occur, and the intensities of these relative to the parent zero-phonon electronic line is[19]

$$P^n = \frac{1}{n!} \left(\frac{m w_k (\alpha_0^{(k)})^2}{\hbar} \frac{2\beta_k^2}{(1+\beta_k^2)^2} \right)^n ,$$

where P^n is the transition probability for the vibronic transition involving n local-mode phonons and β_k is the ratio of the frequency of the kth normal mode in the excited state to that in the ground state, $\beta_k = w_k'/w_k$.

The relative intensities of the local-mode vibronic lines in the absorption spectra are given in Table III. In the fluorescence spectra they are less, typically $\frac{1}{10}$ of the parent electronic lines. From the absorption spectra data, the displacements $\alpha_0^{(Z)}$ of the hydride-, deuteride-, and tritide-ion equilibrium positions in the excited state relative to the ground-state configuration are found to be 0.18, 0.16, and 0.15 Å, respectively, for the calcium fluoride crystals, and 0.27, 0.20, and 0.16 Å for the strontium fluoride crystals. The corresponding fluoride-ion shifts are slightly smaller, being 0.12 and 0.13 Å for calcium and strontium fluoride, respectively.

It is apparent that the shifts $\alpha_0^{(Z)}$ experimentally observed are physically reasonable. The model also shows that the one local-mode vibronic line observed corresponds to the Z vibration mode of the hydride ion.

V. ISOTOPE AND VIBRONIC SHIFTS

Corresponding deuterated and tritiated crystals of calcium and strontium fluoride containing cerium show electronic lines with frequencies slightly different from those in the crystals containing hydrogen. Crystals heated in a mixed hydrogen-deuterium atmosphere display both lines. Such displacements constitute the electronic line isotope shift between hydrogen and deuterium. Similarly, the displacement in frequency in going from hydrogen to tritium constitutes the electronic line isotope shift between hydrogen and tritium.

The local-mode vibronic spectrum yields vibrational intervals corresponding to the localized mode frequencies of hydrogen, deuterium, and tritium coupled to the rare-earth electronic states and these will differ for the various states. The discrepancy between the local-mode frequencies deduced from the vibronic spectra and from those observed directly in the infrared constitutes the local-mode vibronic shift of the excited-state electronic level relative to the ground-state electronic level.

The electron-phonon interaction V_{ev} causes a shift in each electronic level of the cerium ion and all the modes of a lattice contribute to this shift. The isotope shift between hydrogen and deuterium or tritium is the difference in this shift when deuterium or tritium is substituted for hydrogen. It can be assumed that the lattice modes are unaffected by whether hydrogen, deuterium, or tritium is present since these have local-mode frequencies well above the highest optical frequency of the crystal. This is confirmed by the identical lattice-phonon sideband structure observed associated with hydrogen- and deuterium-site electronic lines. Thus the lattice modes contribute equally to the electronic level shift for hydrogen, deuterium, or tritium and their contribution to an isotope shift is zero.

Both the electronic line isotope shifts and local-mode vibronic shifts can arise through the coupling of the localized-mode vibrations to the electronic states of the cerium ion. The widely different zero-point amplitude of vibration for hydrogen, deuterium, and tritium results in different perturbations of the cerium-ion electronic states.

No temperature dependence of the isotope shifts is expected from the electron–local-mode-phonon interaction model since the energies of the local modes are large compared to kT over the temperature range the spectra were measured; the observed isotope shifts are equal at 77 and 4 °K being 24 ± 1 cm^{-1} at 80 °K, 23.6 ± 0.2 cm^{-1} at 40 °K, and 23.8 ± 0.2 cm^{-1} at 12 °K for the calcium fluoride crystals.

The formulation of the electron–local-mode-phonon interaction in the Born-Oppenheimer approximation proceeds as follows: The total wave function $\Psi_{in}(r, Q)$ for the rare-earth–hydride-ion system can be written as a Born-Oppenheimer product of an electronic wave function $\varphi_i(r, Q)$ and a nuclear wave function $\psi_{in}(Q)$. The Hamiltonian for the elec-

tronic wave function includes the electron-phonon interaction V_{ev} given previously in Sec. III and the electronic energy eigenvalues are

$$E_i(X, Y, Z) = E_i + \langle \varphi_i | V_{ev} | \varphi_i \rangle ,$$

where E_i are the electronic energies in the absence of the electron-phonon interaction. The nuclear motion is that of an anharmonic oscillator in the potential of the average electronic energies, and has the Hamiltonian

$$H(X, Y, Z) = T_{kn} + \tfrac{1}{2} m w_Z^2 Z^2 + \tfrac{1}{2} m w_X^2 (X^2 + Y^2) + cZ^3 + dZ(X^2 + Y^2) + \langle \varphi_i | f_z | \varphi_i \rangle Z + \langle \varphi_i | g_{zz} | \varphi_i \rangle Z^2 + \langle \varphi_i | g_{xx} + g_{yy} | \varphi_i \rangle \tfrac{1}{2} (X^2 + Y^2) ,$$

where the T_{kn} are the oscillator kinetic-energy terms. The effect of the electron-phonon interaction results in a shift in the potential minima of the oscillator. The equilibrium condition $\partial V / \partial Z = 0$ yields this displacement in the z direction as approximately $\langle \varphi_i | f_Z | \varphi_i \rangle / m w^2$, and the corresponding potential energy minimum as

$$V_0 \simeq 3 | \langle \varphi_i | f_Z | \varphi_i \rangle |^2 / 2 m w_Z^2 .$$

The total energies of the combined electron-phonon system to second-order terms are thus

$$E_{i n_x n_y n_z} = E_i + (n_x + n_y + n_z + \tfrac{3}{2}) \hbar w + \frac{| \langle \varphi_i | f_Z | \varphi_i \rangle |^2}{2 m w_Z^2} + (n_z + \tfrac{1}{2}) \frac{\hbar \langle \varphi_i | g_{zz} | \varphi_i \rangle}{m w_z} + (n_x + n_y + 1) \frac{\hbar \langle \varphi_i | g_{xx} + g_{yy} | \varphi_i \rangle}{2 m w_x} - 3(n_z + \tfrac{1}{2}) \frac{\hbar c \langle \varphi_i | f_Z | \varphi_i \rangle}{m^2 w_z^3} - (n_x + n_y + 1) \frac{\hbar d \langle \varphi_i | f_Z | \varphi_i \rangle}{m^2 w_x w_z^2} , \quad (11)$$

where $E_{i n_x n_y n_z}$ is the energy of the vibronic level corresponding to the ith electronic state and the $(n_x n_y n_z)$ local-mode phonon state.

A. Electronic Line Isotope Shift

The energies E_{i000} of the zero-phonon levels of the coupled electron–local-mode-phonon system depend on several terms whose values are different for hydrogen, deuterium, and tritium and which thus contribute to an electronic line isotope shift. These terms arise in the following ways:

(a) The electron–local-mode-phonon interaction gives energy shifts through its first-degree terms acting in second-order perturbation, which are, according to (11),

$$| \langle \varphi_i | f_k | \varphi_i \rangle |^2 / 2 m w_k^2 ;$$

but these do not contribute to an isotope shift, since the force constant $m w_k^2$ is the same for hydrogen, deuterium, and tritium.

(b) The electron–local-mode-phonon interaction can produce energy shifts different for hydrogen, deuterium, and tritium through its second-degree terms acting in first-order perturbation, which is according to (11),

$$\frac{\hbar \langle \varphi_i | g_{zz} | \varphi_i \rangle}{2 m w_z} + \frac{\hbar \langle \varphi_i | g_{xx} + g_{yy} | \varphi_i \rangle}{2 m w_x} .$$

(c) The electron–local-mode-phonon interaction can produce energy shifts through the terms involving the anharmonic constants c and d of the potential well in which the hydrogen, deuterium, and tritium ions vibrate. As a result of this anharmonicity, these ions occupy slightly displaced positions in the lattice, and their respective electronic energies differ, according to (11):

$$\frac{\hbar}{2 m w_z} \frac{-3c \langle \varphi_i | f_z | \varphi_i \rangle}{m \omega_z^2} + \frac{\hbar}{2 m w_x} \frac{-2d \langle \varphi_i | f_z | \varphi_i \rangle}{m w_z^2} .$$

(d) Terms involving two close electronic levels φ_1 and φ_2, with energy separation E, can give contributions which may be calculated by perturbation theory if the electron-phonon interaction is small compared to the energy of the local-mode phonons; the result is

$$\frac{\hbar}{2 m w_x} \frac{| \langle \varphi_i | f_x | \varphi_i \rangle |^2}{E + \hbar w_x} + \frac{\hbar}{2 m w_z} \frac{| \langle \varphi_i | f_z | \varphi_i \rangle |^2}{E + \hbar \omega_z} .$$

However, the separation of the energy levels of the $5d^1$ configuration of cerium are sufficiently large for these contributions to be negligible compared to those given earlier, as will be shown in Sec. IV.

The net electronic line isotope shift for the $|\epsilon\rangle$ $5d$ electronic state of cerium thus involves the difference in value for hydrogen, deuterium, and tritium of

$$\delta = \frac{\hbar}{2 m w_z} [\epsilon | z | \epsilon] + \frac{\hbar}{2 m w_x} [\epsilon | x | \epsilon] , \quad (12)$$

where

$$[\epsilon | z | \epsilon] = \left(\langle \epsilon | g_{zz} | \epsilon \rangle - \frac{3c \langle \epsilon | f_z | \epsilon \rangle}{m w_z^2} \right) , \quad (13)$$

$$[\epsilon | x | \epsilon] = \left(\langle \epsilon | g_{xx} + g_{yy} | \epsilon \rangle - \frac{2d \langle \epsilon | f_z | \epsilon \rangle}{m w_z^2} \right) , \quad (14)$$

and $|\epsilon\rangle$ is the $5d$ electronic state of cerium given by (9).

The tritium results are in agreement with this model for the zero-point origin of the isotope shift. In view of the nearly equal values of w_z and w_x, all electronic effects should approximately cancel in the following ratio:

$$\frac{\text{Hydrogen-to-tritium shift}}{\text{Hydrogen-to-deuterium shift}} = \frac{1-M_H w_H/M_T w_T}{1-M_H w_H/M_D w_D} = 1.44$$

using the infrared frequency values. The experimental ratios for comparison are 1.47 and 1.56 for the 3417- and 3370-Å lines of cerium in calcium fluoride and 1.46 for the 3245-Å line of cerium in strontium fluoride. The agreement is quite good and the fact that the experimental values are all slightly larger than 1.44 is in agreement with the tritium modes not being as localized as those of hydrogen or deuterium. The reduction of the tritium amplitude below that of a purely localized mode results in a greater relative isotope shift for tritium.

B. Local-Mode Vibronic Shifts

The local-mode vibronic shift for a local-mode vibronic transition involving n local-mode phonons is given by the energy difference $E_{in}-E_{i0}$ and is made up of three terms:

(i) The first-degree terms of the electron–local-mode-phonon interaction acting in second order give no contribution to the vibronic shift as the terms

$$|\langle\varphi_i|f_k|\varphi_i\rangle|^2/2mw_k^2$$

do not depend on n.

(ii) The second-degree terms of the electron–local-mode-phonon interaction acting in first-order perturbation. For the Z local-mode vibronic transitions, the shift is

$$\frac{n\hbar}{mw_z}\langle\varphi_i|g_{zz}|\varphi_i\rangle$$

and for the X, Y local-mode vibronic transitions, the shift is

$$\frac{n\hbar}{2mw_x}\langle\varphi_i|g_{xx}+g_{yy}|\varphi_i\rangle ,$$

where n is the number of local-mode phonons involved in the local-mode transition.

(iii) The anharmonic terms of the electron–local-mode-phonon interaction give shifts of

$$-\frac{\hbar}{mw_z}\left(\frac{3c\langle\varphi_i|f_z|\varphi_i\rangle}{mw_z^2}\right), \quad -\frac{\hbar}{2mw_x}\left(\frac{2d\langle\varphi_i|f_z|\varphi_i\rangle}{mw_x^2}\right)$$

for the z and x, y vibronics, respectively.

(iv) For two close electronic levels φ_1 and φ_2 with energy separation E, the contribution for a one local-mode vibronic transition is

$$\frac{\hbar|\langle\varphi_i|f_k|\varphi_j\rangle|^2}{2mw_k}\left(\frac{1}{E-\hbar w}+\frac{1}{E+\hbar w}\right).$$

However, as will be shown in Sec. VI, this contribution is small for the energy-level separations appropriate for cerium, so may be neglected.

In the cerium spectra, local-mode vibronics corresponding to the Z vibration of the hydride ion are observed (Table III). The net local-mode vibronic shift δ_{zn} for these vibronic lines is

$$\delta_{zn}=\frac{n\hbar}{mw_z}[\epsilon|z|\epsilon] , \tag{15}$$

where $[\epsilon|z|\epsilon]$ is defined in (13). The corresponding net local-mode vibronic shift δ_{xn} for the x, y vibration of the hydride ion would be

$$\delta_{xn}=\frac{n\hbar}{2mw_z}[\epsilon|x|\epsilon] . \tag{16}$$

The ratio of the hydrogen-to-deuterium shifts is 1.37 as compared to $M_D w_D/M_H w_H = 1.44$. Similarly the hydrogen-to-tritium shift is 1.55 compared to $M_T w_T/M_H w_H = 1.78$. The deviation of the observed ratios from those calculated is expected to be to larger than to smaller values due to the greater degree of localization of the hydrogen vibration compared to those of deuterium and tritium, as found earlier for the electronic line isotope shift. The value of $[\epsilon|z|\epsilon]$ is calculated to be 7×10^3 erg/cm^2 for calcium fluoride.

For strontium fluoride, both the electronic line isotope shift and the vibronic shifts are larger by a factor of 1.41. This increase is partially explained by the lower frequencies of the localized modes in strontium fluoride and by an increase in $[\epsilon|z|\epsilon]$ to 8.3×10^3 erg/cm^2.

C. Assignment of Vibrational Progressions Observed in Cerium Sites of the Parent Crystal

The values of $[\epsilon|z|\epsilon]$ obtained can be used to determine the expected local-mode vibronic shift for the fluoride-ion site lines present in the parent crystals.

The strongest line in the absorption spectrum of the parent calcium fluoride crystal containing cerium is the line at 3131.9 Å which arises from cerium ions in a site of tetragonal symmetry where charge compensation is by a fluoride ion in an empty interstitial cell (Fig. 1). The vibronic sidebands of this line show a 478-cm^{-1} vibrational progression in the fluorescence spectrum and a 484 cm^{-1} in the absorption spectrum. The fluorescence spectrum gives the local-mode frequency associated with the ground-state electronic level while the absorption spectrum gives the local-mode frequency as modified by the electron-phonon interaction in the excited state. If one assumes a localized vibration of the fluoride interstitial ion, in analogy to the hydride, deuteride, and tritide interstitial ions, then the local-mode vibronic shift is expected to be 13 cm^{-1} which is in fair agreement with the observed vibronic shift of 6 cm^{-1}, and supports the proposition that the 475-cm^{-1} frequency is that of

a localized mode of the interstitial fluoride ion in the calcium fluoride lattice.

An analogous result is obtained for strontium fluoride crystals containing cerium. The difference in the observed vibrational progression frequencies is 14 cm^{-1} while the value expected from extrapolation from the hydrogen, deuterium, and tritium results is 18 cm^{-1}.

For the barium fluoride crystals containing cerium, the hydrogenic spectra show no resolved fine structure even at 2 °K. The parent crystals show the fluoride-ion vibronic frequencies as 398 cm^{-1} in fluorescence and 403 cm^{-1} in absorption so the vibronic shift and hence the electron-phonon interaction effects in barium fluoride are similar to those in the other alkaline-earth fluorides.

The X, Y components of the localized hydrogen-, deuterium-, and tritium-ion vibrations were not detected in the cerium vibronic spectra. However, internal consistency of the expressions for the shifts δ, δ_{z1}, and δ_{x1} given by (12), (15), and (16) require the X, Y vibronic shifts to be 30 and 42 cm^{-1} for calcium and strontium fluoride, respectively, which are about 0.3 of the corresponding Z vibronic shifts.

VI. POINT-CHARGE MODEL FOR ELECTRONIC ISOTOPE SHIFTS AND LOCAL-MODE VIBRONIC SHIFTS

The experimentally observed electronic line isotope shift is the difference in isotope shift for the two electronic states involved in the transition. For the several cerium-ion interconfigurational transitions investigated in fluorescence (Table II), the one common emitting state is the lowest crystal field level of the $5d$ configuration, and the terminating states comprise crystal field components of the $^2F_{5/2}$ and $^2F_{7/2}$ multiplets of the $4f^1$ configuration. The isotope shifts of all these transitions are the same to within 2 cm^{-1} so the principal part of the observed isotope shift can be attributed to electron-phonon interaction effects in the $5d$ electronic state.

The experimentally observed local-mode vibronic shift is the difference in vibronic shift between the excited and ground electronic states. The shifts are nearly all the same for the various electronic states of the $4f^1$ configuration and are small so, as in the case of the electronic line isotope shifts, the observed vibronic shifts must be attributed primarily to electron-phonon interactions in the $5d$ electronic state.

The lowest $5d$ electronic state φ of cerium in a tetragonal C_{4v} symmetry crystal field is the cubic-field $|\epsilon\rangle$ wave function given in (9).

It is required to evaluate the matrix elements of the g_{zz}, $g_{xx}+g_{yy}$, and f_z electronic functions for this cerium-ion electronic state, and to determine the cubic anharmonic constants c and d.

Two simple models for the electron–local-mode-phonon interaction are the point-charge and dipole models introduced in Sec. III, and the electronic coordinate functions f_x, f_y, f_z, g_{zz}, $g_{xx}+g_{yy}$, $g_{xx}-g_{yy}$, g_{xy}, g_{yz}, and g_{xz} for these models are given in the Appendix. The nonvanishing matrix elements of the electronic functions g_{zz} and $g_{xx}+g_{yy}$ for the cerium $|\epsilon\rangle$ wave function are

$$\langle\epsilon|g_{zz}|\epsilon\rangle = -\langle\epsilon|g_{xx}+g_{yy}|\epsilon\rangle = \frac{-12eq\langle r^2\rangle}{7D^5} + \frac{5eq\langle r^4\rangle}{7D^7}$$

for the point charge, and

$$\langle\epsilon|g_{zz}|\epsilon\rangle = \frac{-60ep\langle r^2\rangle}{7D^6} + \frac{5ep\langle r^4\rangle}{D^8},$$

$$\langle\epsilon|g_{xx}+g_{yy}|\epsilon\rangle = \frac{6ep\langle r^2\rangle}{D^6} - \frac{80ep\langle r^4\rangle}{21D^8}$$

for the dipole model, where $\langle r^n\rangle$ is the average value of r^n for the cerium $5d$ orbital and is taken as 7.00 a.u. and 70.66 a.u. for $\langle r^2\rangle$ and $\langle r^4\rangle$, respectively, in the following numerical calculations.

The nonvanishing matrix element of the f_z electronic coordinate function for the cerium ϵ wave function is

$$\langle\epsilon|f_z|\epsilon\rangle = \frac{6eq\langle r^2\rangle}{7D^4} - \frac{5eq\langle r^4\rangle}{21D^6}$$

for the point-charge model, and

$$\langle\epsilon|f_z|\epsilon\rangle = \frac{24ep\langle r^2\rangle}{7D^5} - \frac{10ep\langle r^4\rangle}{7D^7}$$

for the dipole model.

The cubic anharmonic constants c and d may be estimated from the infrared local-mode spectra in the following way: The anharmonic terms of the potential well cause shifts in the frequencies of the local modes of the light ions and also allow observation of harmonics of them. Because these terms are relatively small, their effect may be estimated by perturbation theory and this has been done by Maradudin and Peretti[20] to first order in the quartic terms and to second order in the cubic terms since both are comparable contributions; having the same ratio of displacement to interionic distance. The frequency shift of the second-harmonic lines from twice the fundamental frequencies yields three equations in the six anharmonic constants c, d, f, g, h, and k:

$$E(002) - 2E(001) = 12\beta^4 g - \frac{60c^2\beta^6}{\hbar w_z},$$

$$E(101) - [E(100) + E(001)] = 4h\alpha^2\beta^2 - \frac{12cd\beta^4\alpha^2}{\hbar w_z} - \frac{16d^2\alpha^4\beta^2}{\hbar w_x[4-(w_z/w_x)^2]},$$

$$E(200) - 2E(100) = 2\alpha^4(k + 6f) + \frac{16d^2\beta^4\alpha^2[2 - (w_z/w_x)^2]}{\hbar w_x[4 - (w_z/w_x)^2]} ,$$

where $\alpha = (\hbar/2mw_x)^{1/2}$, $\beta = (\hbar/2mw_z)^{1/2}$ and $E(nmp)$ is the energy of the (nmp) state.

Three second-harmonic transitions are expected and have been observed[1] for calcium fluoride crystals containing gadolinium, thulium, and yttrium. The observation of the corresponding transitions in the crystals containing cerium is confused by the presence of overlying absorption due to the $^2F_{5/2} \rightarrow {}^2F_{7/2}$ electronic transitions of cerium in the 2000-cm^{-1} region. The frequencies of these second-harmonic transitions can, however, be estimated to within 10 cm^{-1} by extrapolation from the gadolinium, thulium, and yttrium values to be 1975, 2110, and 2240 cm^{-1}. The frequency shifts of the second-harmonic lines from twice the fundamental frequencies are all negative which requires the quartic anharmonic constants g, h, and $k + 6f$ to be negative. As an upper limit, the contribution of the cubic terms is set to equal the observed anharmonic shifts, which yields

$$|c| \leq 2\times 10^{12} \text{ erg/cm}^3 , \quad |d| \leq 3.5\times 10^{12} \text{ erg/cm}^3 .$$

An alternative estimate of the value of these anharmonic constants c and d can be made from the point-charge and dipole-model expressions given by Eq. (7) and (8). For $q = \sigma = 0.85e$ and $p/e = 1.1$ Bohr radii,

$$c = 6\times 10^{11} \text{ erg/cm}^3 , \quad d = 6.5\times 10^{11} \text{ erg/cm}^3 .$$

These are taken as the values for the following numerical calculations.

The shift in equilibrium position of the hydrogen, deuterium, and tritium ions from the center of the harmonic potential due to these cubic anharmonic terms is

$$\langle 000' | z | 000' \rangle = \frac{6c\beta^4}{\hbar w_z} + \frac{4d\alpha^2\beta^2}{\hbar w_x} ,$$

which is 0.006, 0.004, and 0.003 Å for hydrogen, deuterium, and tritium, respectively.

The shift in the first z vibronic line is, according to (15),

$$\delta_{z1} = \frac{\hbar}{mw_z}[\epsilon | z | \epsilon] .$$

For $w_z = 1130$ cm^{-1} and $e = q = 0.85$ of the electronic charge, the point-charge-model value for δ_{z1} is -60 cm^{-1}, and the dipole-model value is -66 cm^{-1}.

The shift δ in the zero-phonon electronic line is according to (12),

$$\delta = \frac{\hbar}{2mw_z}[\epsilon | z | \epsilon] + \frac{\hbar}{2mw_x}[\epsilon | x | \epsilon].$$

The isotope shift consists of the difference in this shift in going from hydrogen to deuterium, and for $w_x = 990$ cm^{-1} and $w_z = 1130$ cm^{-1} for hydrogen the point-charge value of $(\delta_H - \delta_D)$ is -3.1 cm^{-1} and the dipole-model value is -5.7 cm^{-1}. In both cases, both models give values that are of opposite sign to those observed.

The first-degree terms f_x, f_y, and f_z can contribute in second-order perturbation via the other $5d$ electronic states of the cerium ion. Of these, the second E_g level which has the cubic field wave function $|\theta\rangle$ has zero matrix elements with $|\epsilon\rangle$ while the three levels of the $|5d, T_{2g}\rangle$ state are 8000 cm^{-1} away and their total contribution to the Z vibronic frequency shift is ~ 2 cm^{-1} which is negligible compared to the contribution from the second-degree g_{zz} terms.

Both the point-charge and the dipole model are thus incapable of explaining the sign of either the observed Z vibronic frequency shift or the observed zero-phonon electronic line isotope shift, and it is necessary to consider other mechanisms to explain these effects.

The four fluorine ions between the cerium ion and the hydride ion can influence electronic line isotope shifts and vibronic shifts in the following ways.

(a) The motion of the hydride and deuterium ions can induce motion of the four fluorine ions at their local-mode frequencies. The deuterium ion will drive the four fluorine ions with larger amplitude since its local-mode frequency is closer to the lattice frequencies. Calculations on a model of four point-charge fluorine ions being driven by a vibrating hydride ion show that to account for the observed magnitude of the isotope shifts the hydride ion must drive the four fluorine ions from $\frac{1}{10}$ to $\frac{1}{4}$ of the mean-square amplitude typical of a normal vibrational mode of a four fluorine-ion complex. However, the value of 1.38 for the ratio of the hydrogen-to-deuterium local-mode frequencies sets the upper limit for the amplitude of the neighboring fluorine ions as $\frac{1}{50}$, so this mechanism is not capable of explaining the magnitude of the observed electron-phonon effects.

(b) The motion of the hydride ion induces a dipole moment on the four fluorine ions through the short-range repulsive forces between these ions. This so-called distortion dipole moment can follow the rapid hydrogen or deuterium ion motion because it is a purely electronic effect and does not require the fluorine nuclei to vibrate at the local-mode frequencies. A point-charge model for this interaction yields values for the f_z, g_{zz}, and $g_{xx} + g_{yy}$ electronic coordinate functions which are given in the Appendix. For the case of the hydride and fluorine ions located in the lattice positions of the undistorted calcium fluoride lattice,

$$\langle \epsilon | g_{zz} | \epsilon \rangle = \frac{-2^{11}\times 0.7\alpha eq}{3^6 D^8} T_2^0 ,$$

$$\langle \epsilon | f_z | \epsilon \rangle = \frac{2^{10} \alpha e q}{3^5 D^7} T_2^0 ,$$

$$\langle \epsilon | g_{xx} + g_{yy} | \epsilon \rangle = \frac{-2^9 \times 0.25 \alpha e q}{3^6 D^8} T_2^0 ,$$

where α is the polarizability of the fluorine ions and T_2^0 is defined in the Appendix. For $\alpha = 0.99$ Å^3,[10] these values become

$$\langle \epsilon | g_{zz} | \epsilon \rangle = -0.96 \frac{eq}{D^5} T_2^0 ,$$

$$\langle \epsilon | f_z | \epsilon \rangle = +0.21 \frac{eq}{D^4} T_2^0 ,$$

$$\langle \epsilon | g_{xx} + g_{yy} | \epsilon \rangle = -1.7 \frac{eq}{D^5} T_2^0 .$$

$\langle \epsilon | g_{zz} | \epsilon \rangle$ is about $\frac{1}{6}$ and of opposite sign to the direct-interaction point-charge value. Similarly, $\langle \epsilon | f_z | \epsilon \rangle$ is about $\frac{1}{15}$ and of opposite sign to the point-charge direct-interaction value. The net shift δ_{z1} in the first Z vibronic line is thus $+9.7$ cm^{-1}. $\langle \epsilon | g_{xx} + g_{yy} | \epsilon \rangle$ is of the same sign as the point-charge direct-interaction value, and the electronic line isotope shift δ is $+6.1$ cm^{-1}.

A refinement to the model is to include the effect of the change in the environment of the cerium and hydride ions caused by the change in the position of the surrounding fluorine ions, as postulated by Kiro and Low[21] on the basis of ENDOR measurements. If the four fluorine ions between the cerium and hydride ion are displaced 0.15 Å outwards along the hydride-fluorine ion directions, then

$$\langle \epsilon | g_{zz} | \epsilon \rangle = -0.91 \frac{eq}{D^5} T_2^0 ,$$

$$\langle \epsilon | f_z | \epsilon \rangle = +0.26 \frac{eq}{D^4} T_2^0 ,$$

$$\langle \epsilon | g_{xx} + g_{yy} | \epsilon \rangle = -1.0 \frac{eq}{D^5} T_2^0 ,$$

while if the equilibrium position of the hydride ion is also moved 0.1 Å towards the cerium ion, then

$$\langle \epsilon | g_{zz} | \epsilon \rangle = -1.0 \frac{eq}{D^5} T_2^0 ,$$

$$\langle \epsilon | f_z | \epsilon \rangle = +0.29 \frac{eq}{D^4} T_2^0 ,$$

$$\langle \epsilon | g_{xx} + g_{yy} | \epsilon \rangle = -1.2 \frac{eq}{D^5} T_2^0 .$$

These changes indicate that distortions of the calcium fluoride lattice of the magnitude postulated by Kiro and Low are not very significant in influencing the calculated values of the electron-phonon interaction effects.

The participation of the four fluorine ions in the cerium-hydride ion interaction thus gives a contribution whose sign is in agreement with observation, but whose magnitude is smaller than required.

The several contributions to the electronic line isotope shift and to the z vibronic isotope shift comprise (a) the point-charge interaction between the cerium ion and the hydride ion, (b) the dipole moment interaction between the cerium ion and the hydride ion, and (c) the interaction via the polarization of the four fluorine ions between the cerium and hydride ion. The net electronic line isotope shift is -4.7 cm^{-1} and the net z vibronic line shift is -115 cm^{-1}, which are comparable to the observed values, but of the wrong sign.

It can be concluded that purely electrostatic models for the electron-phonon interaction are unable to quantitatively explain the sign of the observed shifts. Nevertheless, these models are of some value in that they indicate the relative importance of the several contributions to these shifts. In particular, the effect of the four fluorine ions in influencing isotope shifts has been shown to be significant; and in more sophisticated models involving overlap effects between the ions, this interaction through the fluorine ions is expected to be the predominant one determining the magnitude and sign of the electron-phonon interaction effects in the optical spectra. It is not feasible with the present data on the cerium system to attempt to develop covalency models for the cerium-ion system. Instead, more experimental investigations would appear to be desirable to determine the effect of change in site symmetry and charge state of the hydride ion on the sign and magnitude of the electron-phonon interaction effects. The importance of these changes is shown by the preliminary data for the cerium site characterized by the doublet at 3355.6 and 3357.2 Å. This has a reversed electronic line isotope shift but the same z vibronic frequency shift as the principal C_{4v} symmetry site (Table II).

The cerium-ion system is a convenient system for these studies because of the large magnitude of electron-phonon interaction effects in transitions to and from $5d$ electronic states.

VII. LATTICE VIBRONIC SPECTRUM

Table VIII lists the observed lattice vibration frequency intervals observed in the ultraviolet absorption spectrum of the hydrogenated and deuterated calcium fluoride crystals (Figs. 8 and 9). The lattice frequencies of the host lattice are also listed where appropriate, and these frequencies taken singly or in combination yield the assignment of the lattice vibronic spectra shown. Of the unassigned lines, those in the low-frequency region correspond to peaks in the phonon density of states which involve the acoustic lattice vibrations. The corresponding strontium fluoride data may be compared with the data of Cohen and Guggenheim[22] and Richman.[23]

The vibronic spectra of the hydrogen, deuterium, and tritium sites in the calcium fluoride crystals

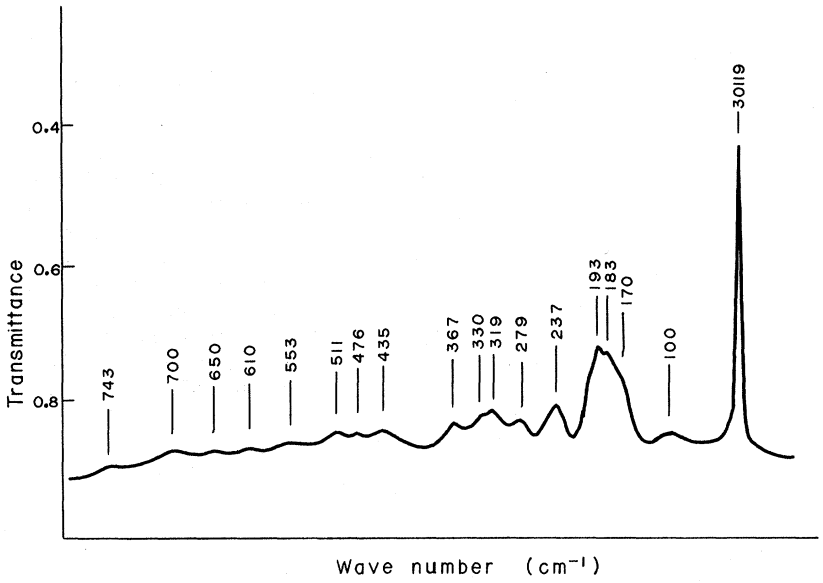

FIG. 8. First local-mode vibronic of deuterium and its associated lattice phonon sideband as observed in a deuterated crystal of calcium fluoride containing 0.05% cerium. The separations of the lattice phonon peaks from the parent transition are shown in cm^{-1}.

show no evidence for the 484-cm^{-1} vibrational progression which is such a characteristic feature of the normal tetragonal cerium site. Similarly, the 438-cm^{-1} progression observed for the tetragonal sites of cerium in strontium fluoride crystals is absent in the vibronic spectra of the hydrogen-, deuterium-, and tritium-site spectra. These progression frequencies have been postulated by Kapalanskii to be localized vibration modes, but the nature of such modes was not elucidated. On the basis of the correspondence with the hydride-ion local modes, they are assigned as localized vibration modes of the fluoride interstitial ion associated with the tetragonal cerium site.

In this vibration mode, the fluoride ion may be considered to be partaking in the same Z type of vibration as the hydride ion in its local-mode vibration; but, because of the larger mass of the fluoride ion, the vibration is no longer well localized for this ion and the surrounding neighbor ions also vibrate in the mode.

The appearance of vibronic transitions arises through the coupling of the cerium-ion electronic states to the phonon system through the linear part of the electron-phonon interaction. Bron[17] has shown that interconfigurational transitions couple primarily to vibrations of the lattice in the immediate vicinity of the optically active ion and the resultant vibronic spectra are dominated by transitions to vibrational modes of a high local amplitude. Intraconfigurational electronic transitions, on the other hand, yield vibronic spectra reflecting the phonon spectra of the host lattice.

The cerium transitions here are interconfigurational and show the expected local-mode-type vibrational progressions on which are superposed the phonon spectra of the host lattices. Wagner and Bron[24] have interpreted the largest vibrational progression frequency to be the resonance frequency of a pseudolocalized vibration, whose value is slightly greater than the longitudinal-optical-branch frequency at $\vec{k}=0$ of the host lattice. The fluoride-ion local-mode frequencies have been determined to be 478, 424, and 398 cm^{-1} for calcium, strontium, and barium fluoride, respectively, and these values may be compared with the corresponding longitudinal-optical-branch frequencies at[25,26] $k=0$ of 463, 374, and 326 cm^{-1}, respectively for the three host lattices.

TABLE VIII. Assignment of the lattice frequency vibronics observed in hydrogenated and deuterated crystals of calcium fluoride containing 0.05% cerium. Crystal temperature 12 °K.

Assignment	Frequency	Observed line frequency (average of values of Table IV)
	• • •	100
	• • •	169
	• • •	182
	• • •	192
	• • •	237
LO_2	286[a]	282
$k=0$ Raman[a]	321	319
TO_2	325[a]	332
LO_1	368[a]	367
LO_2+TA	431	434
TO_2+TA, LO_1 at $k=0$[a]	463[a]	474
LO_1+TA	516	512
LO_2+LO_2	564	558
LO_2+TO_2	614	612
LO_2+LO_1	649	652
LO_1+TO_2	700	700
LO_1+LO_1	734	747

[a]Data of Fray *et al.* (Ref. 25).

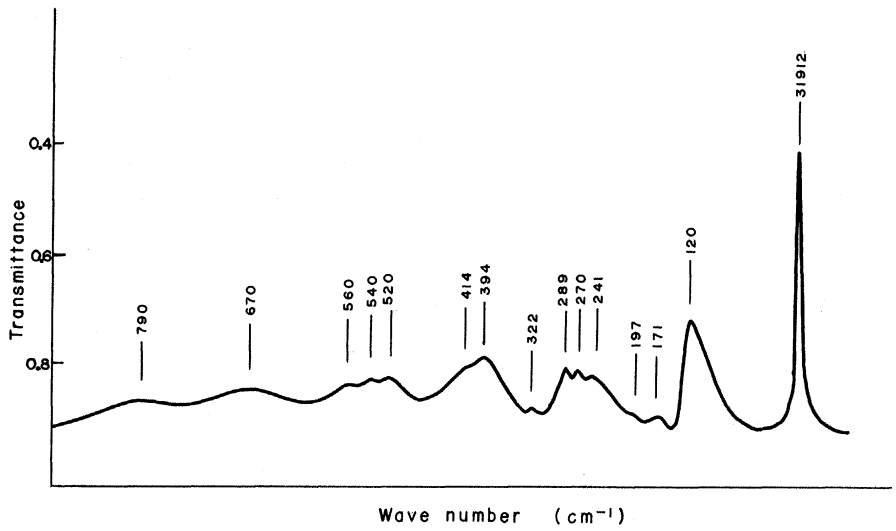

FIG. 9. First local-mode vibronic transition of hydrogen and its associated lattice phonon sideband as observed in a hydrogenated crystal of strontium fluoride containing 0.05% cerium. The separations of the lattice phonon peaks from the parent transition are shown in cm^{-1}.

ACKNOWLEDGMENT

The authors are grateful to Professor B. G. Wybourne for his sincere interest and encouragement in this work.

APPENDIX

The electron–local-mode-phonon interaction appropriate for the C_{4v}-symmetry cerium-hydride ion pair was shown in Sec. III to have the form

$$V_{ev} = f_x X + f_y Y + f_z Z + \tfrac{1}{2}(g_{xx}+g_{yy})(X^2+Y^2) + \tfrac{1}{2}(g_{xx}-g_{yy})(X^2-Y^2) + g_{xx}XY + g_{xz}XZ + g_{yz}YZ + g_{zz}Z^2 .$$

This interaction is the difference between the crystal field for an arbitrary displacement of the light ion and the crystal field for equilibrium. If overlap and covalency effects are neglected, the crystal field potential of the cerium ion's electron in the field of the hydride ion can be expressed in terms of the solid harmonics defined as follows:

$$T^m_{n,x} = r^n P^m_n(\cos\theta)\cos m\varphi,$$
$$T^m_{n,y} = r^n P^m_n(\cos\theta)\sin m\varphi,$$

where r, θ, and φ are the spherical polar coordinates for the cerium ion's electron, n and m are positive integers with $m \leq n$, and the $P^m_n(x)$ are the Legendre polynomials, defined by

$$P^m_n(x) = (-1)^m \left(\frac{1}{2^n n!}\right)(1-x^2)^{m/2}\frac{d^{(n+m)}}{dx^{(n+m)}}(x^2-1)^n,$$

where $x = \cos\theta$.

The following relationships for the behavior of the solid harmonics T^m_n under differentiation with respect to the Cartesian x, y, z coordinates will be found useful:

$$\frac{\partial}{\partial z}T^m_{n,x} = (n+m)T^m_{n-1,x}\ , \quad \frac{\partial}{\partial z}T^m_{n,y} = (n+m)T_{n-1,y}$$

for $n, m \geq 0$, and

$$2\frac{\partial}{\partial x}T^m_{n,x} = -(n+m)(n+m-1)T^{m-1}_{n-1,x} + T^{m+1}_{n-1,x},$$
$$2\frac{\partial}{\partial x}T^m_{n,y} = -(n+m)(n+m-1)T^{m-1}_{n-1,y} + T^{m+1}_{n-1,y},$$
$$2\frac{\partial}{\partial y}T^m_{n,x} = +(n+m)(n+m-1)T^{m-1}_{n-1,y} + T^{m+1}_{n-1,y},$$
$$2\frac{\partial}{\partial y}T^m_{n,y} = -(n+m)(n+m-1)T^{m-1}_{n-1,x} - T^{m+1}_{n-1,x}$$

for $n \geq 0$, $n \geq 1$, and

$$\frac{\partial}{\partial x}T^0_{n,x} = T^1_{n-1,x}\ , \quad \frac{\partial}{\partial y}T^0_{n,x} = T^1_{n-1,y}$$

for $n \geq 0$ $(m = 0)$. Here it is understood that $T^m_{n,i} = 0$ for $m > n$.

The crystal field potential may be expanded as a Taylor series in the light-ion displacements:

$$V_c = V_{c0} + \sum_i \left(\frac{\partial V_{c0}}{\partial X_i}\right)(\Delta X_i) + \tfrac{1}{2}\sum_{i,j}\frac{\partial^2 V}{\partial X_i\,\partial X_j}\Delta X_i \Delta X_j + \cdots .$$

The electronic functions f_i and g_{ij} of the electron-phonon interaction can thus be obtained by appropriate differentiation of the crystal field potential with respect to the light-ion coordinates.

The electron-phonon interaction involving the light ion alone is axial and transforms as the totally symmetric representation of the $C_{\infty v}$ group while the f_i and g_{ij} electronic functions transform as the same irreducible representations as the corresponding function of the light-ion displacements. By inspection of the $C_{\infty v}$ and C_{4v} group tables, the following relations can be established between the f_i

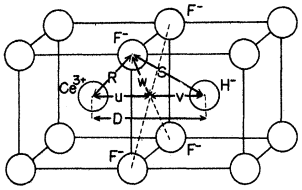

FIG. 10. Schematic representation of the calcium fluoride lattice defining the distances u, v, w, R, and S.

and g_{ij} electronic functions and the solid harmonics T^m_{nx} and T^m_{ny}:

$$f_z = a_{0n} T^0_n, \qquad g_{xz} = b_{0n} T^0_n, \qquad g_{yz} = b_{1n} T^1_{ny},$$
$$f_x = a_{1n} T^1_{nx}, \quad (g_{xx}+g_{yy}) = c_{0n} T^0_n, \quad g_{xx}-g_{yy} = b_{2n} T^2_{nx},$$
$$f_y = a_{1n} T^1_{ny}, \qquad g_{xz} = b_{1n} T^1_{nx}, \qquad g_{xy} = c_{2n} T^2_{ny},$$

where the constants a_{in}, b_{in}, and c_{in} depend on the particular model chosen for the light-ion interaction.

1. Point-Charge Model

The crystal field potential of the cerium-ion electron in the point-charge field of the hydride ion is a function of the difference in the Cartesian coordinates for the electron and the hydride ion, so the following relations hold:

$$\frac{\partial V_c}{\partial X} = \frac{-\partial V_c}{\partial x}, \quad \frac{\partial V_c}{\partial Y} = \frac{-\partial V_c}{\partial y}, \quad \frac{\partial V_c}{\partial Z} = \frac{-\partial V_c}{\partial z}.$$

Using this together with the generating function relation for the Legendre polynomials,

$$(1-2tz+t^2)^{-1/2} = \sum_{k=0} t^k P^0_k(z)$$

yields the following values for the a_{in}, b_{in}, and c_{in} constants:

$$a_{0n} = -(n+1)eqD^{-(n+2)},$$
$$b_{0n} = -c_{0n} = \tfrac{1}{2}(n+1)(n+2)eqD^{-(n+3)},$$
$$a_{1n} = -eqD^{-(n+2)},$$
$$b_{1n} = (n+2)eqD^{-(n+3)},$$
$$b_{2n} = c_{2n} = +eqD^{-(n+3)},$$

where D is the distance between the equilibrium positions of the rare-earth and hydride ions in the lattice, e is the proton charge, and q is the hydride-ion charge. Since the potential satisfies Laplace's equation, the g functions satisfy

$$g_{xx}+g_{yy}+g_{zz} = 0. \tag{17}$$

2. Dipole Models

The electron–light-ion interaction is between the cerium-ion electron and the dipole moment field of the light ion. It is assumed that the dipole moment has a constant magnitude independent of the position of the vibrating light ion and is directed towards the center of the cerium ion. For the x,y vibration of the light ion, the direction of the dipole moment is thus changing during the motion, so Eq. (17) is no longer satisfied. The following values of a_{in}, b_{in}, and c_{in} are calculated:

$$a_{0n} = -(n+1)(n+2)epD^{-(n+3)},$$
$$a_{1n} = -(n+3)epD^{-(n+3)},$$
$$b_{0n} = \tfrac{1}{2}(n+1)(n+2)(n+3)peD^{-(n+4)},$$
$$c_{0n} = -\tfrac{1}{2}(n+1)[(n+1)(n+2)+2]peD^{-(n+4)},$$

where p is the absolute value of the dipole moment of the light ion.

3. Polarization of Fluorine-Ion Model

The electron–light-ion interaction is between the cerium d electron and the point charge of the hydride ion through the dipole moments induced on the four fluorine ions between the cerium and hydride ion. The values of a_{02}, a_{12}, b_{02}, and c_{02} are

$$a_{02} = \frac{2\gamma eq}{R^4S^3}\left[\frac{-4wv}{S^2}P^1_3\left(\frac{u}{R}\right) + 3\left(2-\frac{v^2}{S^2}\right)P^0_3\left(\frac{u}{R}\right)\right],$$

$$a_{12} = \frac{\gamma eqw}{6R^4S^5}\left[wP^2_3\left(\frac{u}{R}\right) + 4vP^1_3\left(\frac{u}{R}\right)\right],$$

$$b_{02} = \frac{-2\gamma eq}{R^4S^5}\left\{\left(\frac{5v^2}{S^2}-1\right)\left[4wP^1_3\left(\frac{u}{R}\right) + 3vP^0_3\left(\frac{u}{R}\right)\right] - 24vP^0_3\left(\frac{u}{R}\right)\right\},$$

$$c_{02} = \frac{2\gamma eq}{R^4S^5}\left[8w\left(\frac{5w^2}{S^2}-3\right)P^1_3\left(\frac{u}{R}\right) + 3v\left(\frac{10w^2}{S^2}-1\right)P^0_3\left(\frac{u}{R}\right)\right],$$

where γ is the polarizability of the fluorine ions; u, v, w are the distances defined by Fig. 10; $R^2 = u^2+w^2$; $S^2 = v^2+w^2$; and the P^m_l are the Legendre polynomials.

---

†Research supported in part by the Air Force Office of Scientific Research, Office of Aerospace Research, U.S. Air Force, under AFOSR Grant No. 1275-67.

*On leave from the Institute of Radio Electronics, Czechoslovak Academy of Science, Prague, Czechoslovakia.

[1]G. D. Jones, S. Peled, S. Rosenwaks, and S. Yatsiv, Phys. Rev. 183, 353 (1969).

[2]G. D. Jones and R. A. Satten, Phys. Rev. 147, 566 (1966).

[3]A. A. Kapalanskii, V. N. Medvedev, and P. P. Feofilov, Opt. i Spektroskopiya 14, 664 (1963) [Opt. Spectry.

(USSR) 14, 351 (1963)].
[4]M. H. Crozier, Phys. Rev. 137, A1781 (1965).
[5]R. C. Newman, Advan. Phys. 18, 545 (1969).
[6]D. N. Chambers and R. C. Newman, Phys. Status Solidi 35, 685 (1969).
[7]S. A. Pollack and R. A. Satten, J. Chem. Phys. 36, 804 (1962).
[8]R. G. Bessent and W. Hayes, Proc. Roy. Soc. (London) A285, 430 (1965).
[9]D. Kiro, W. Low, and A. Kafri, Phys. Rev. Letters 22, 893 (1969).
[10]S. Fraga and G. Malli, *Many Electron Systems: Properties and Interactions* (Saunders, Philadelphia, 1968), p. 84.
[11]N. V. Starostin, Opt. i Spektroskopiya 23, 807 (1967) [Opt. Spectry. (USSR) 23, 437 (1967)].
[12]M. H. Weber and R. W. Bierig, Phys. Rev. 134, A1492 (1964).
[13]J. M. Baker, E. R. Davies, and T. R. Reddy, Phys. Letters 29A, 118 (1969).
[14]S. Peled (private communication).
[15]E. Loh, Phys. Rev. 154, 270 (1967).
[16]W. J. Manthey (private communication).
[17]W. E. Bron, Phys. Rev. 140, A2005 (1965).
[18]K. Rajnak, J. Chem. Phys. 37, 2440 (1962).
[19]M. Wagner, J. Chem. Phys. 41, 3939 (1964).
[20]A. A. Maradudin and J. Peretti, Phys. Rev. 161, 852 (1967).
[21]D. Kiro and W. Low, Phys. Letters 29A, 537 (1969).
[22]E. Cohen and H. J. Guggenheim, Phys. Rev. 175, 354 (1968).
[23]I. Richman, Phys. Rev. 133, A1364 (1964).
[24]M. Wagner and W. E. Bron, Phys. Rev. 139, A223 (1968).
[25]S. J. Fray, F. A. Johnson, and J. E. Quarrington, in *Proceedings of the International Conference on Lattice Dynamics, Copenhagen*, 1963 (Pergamon Press, Oxford, 1965), p. 377.
[26]W. Kaiser, W. G. Spitzer, R. H. Kaiser, and L. E. Howarth, Phys. Rev. 127, 1950 (1962).

PHYSICAL REVIEW B VOLUME 3, NUMBER 9 1 MAY 1971

Nuclear-Magnetic-Resonance Studies of Eu^{151} and Eu^{153} in Europium Iron Garnet Single Crystals

R. L. Streever and P. J. Caplan
Institute for Exploratory Research, U. S. Army Electronics Command, Fort Monmouth, New Jersey 07703
(Received 4 August 1970)

The nuclear magnetic resonances of Eu^{151} and Eu^{153} have been studied at 4.2 °K in single crystals of europium iron garnet with externally applied fields of sufficient magnitude to align the magnetization along various crystallographic directions. Hyperfine field and quadrupole splitting parameters of the Eu^{+3} ions are obtained. Hyperfine fields along the principal orthorhombic axes (x, y, and z) of the rare-earth sites are found to be 649, 706, and 382 kG, respectively, where the z axis corresponds to the orthorhombic axis which lies along the cubic [100] direction. The anisotropy of the hyperfine field is shown to be due in part to the crystal field distortion and in part to the anisotropy of the exchange fields arising from the iron ions. From the Eu^{153} quadrupole splittings, contributions to the electric field gradient arising from the crystal fields and the exchange fields are obtained. Values of the crystal field parameters and anisotropic exchange fields are obtained and discussed in relation to those in other rare-earth iron garnets.

I. INTRODUCTION

In recent years a number of experimental studies[1-4] using the Mössbauer effect as well as theoretical studies[2-6] have been carried out to determine the hyperfine fields and quadrupole interactions of the Eu^{+3} ions in europium iron garnet (EuIG). The Mössbauer studies of pure EuIG, however, have been restricted to "zero fields" where the magnetization is along the easy ⟨111⟩ direction. From studies in this direction only, one cannot obtain independently all three hyperfine field parameters associated with the orthorhombic symmetry at the rare-earth site. We have studied the nuclear magnetic resonance (NMR) of Eu^{151} and Eu^{153} in a single crystal of EuIG with external fields of sufficient magnitude to align the magnetization along the orthorhombic axes of the rare-earth sites and have determined the hyperfine fields and quadrupole splittings. A preliminary account of this study and an account of a zero-field study of the Eu^{151} and Eu^{153} NMR in polycrystalline EuIG were reported previously.[7,8] In the present paper we present results of more extended experimental studies and a more extended discussion of the findings.

As a result of the exchange and crystal fields acting on the Eu^{+3} ion, the $^7F_0$ ground state is mixed with the excited ionic states $^7F_1$ and $^7F_2$. The hyperfine field anisotropy arises from both the anisotropy of the exchange field and from the orthorhombic crystal fields. The hyperfine field parameters and electric field gradients associated with the